Structural Interactions Between Deep Mesozoic Strike-Slip Faults and Shallow Cenozoic Contractional Folds in the Northern Tianshan Foreland Basin (NW China)

Zhenyu Peng, Xin Wang, Fabien Graveleau, Bruno Vendeville, Alan Nunns

Tectonics®

RESEARCH ARTICLE
10.1029/2023TC007986

Structural Interactions Between Deep Mesozoic Strike-Slip Faults and Shallow Cenozoic Contractional Folds in the Northern Tianshan Foreland Basin (NW China)

Zhenyu Peng[1], Xin Wang[1], Fabien Graveleau[2], Bruno C. Vendeville[2], and Alan G. Nunns[3]

[1]School of Earth Science, Zhejiang University, Hangzhou, China, [2]IRD, UMR 8187, LOG, Laboratoire d'Océanologie et de Géosciences, CNRS, Université de Lille, Université du Littoral Côte d'Opale, Lille, France, [3]StructureSolver LLC, Houston, TX, USA

Key Points:

- The geometry and kinematics of Mesozoic transpressional and transtensional structures were documented using 3-D seismic data
- The Mesozoic strike-slip faults affected the localization of Cenozoic thin-skinned folding by creating pinch-out or folds in the *décollement*
- Cenozoic forelandward folding consumed 7 km S-N shortening. Shortening rate decreased from 0.90–1.46 to 0.24–0.37 mm/yr eastward

Supporting Information:

Supporting Information may be found in the online version of this article.

Correspondence to:

X. Wang,
wx@zju.edu.cn

Citation:

Peng, Z., Wang, X., Graveleau, F., Vendeville, B. C., & Nunns, A. G. (2024). Structural interactions between deep Mesozoic strike-slip faults and shallow Cenozoic contractional folds in the Northern Tianshan foreland basin (NW China). *Tectonics*, *43*, e2023TC007986. https://doi.org/10.1029/2023TC007986

Received 27 JUN 2023
Accepted 22 JAN 2024

Author Contributions:

Conceptualization: Zhenyu Peng, Xin Wang, Bruno C. Vendeville
Formal analysis: Zhenyu Peng
Funding acquisition: Xin Wang
Investigation: Zhenyu Peng, Xin Wang
Methodology: Zhenyu Peng, Xin Wang, Alan G. Nunns
Project Administration: Xin Wang
Software: Zhenyu Peng, Alan G. Nunns
Supervision: Xin Wang, Fabien Graveleau
Validation: Zhenyu Peng
Writing – original draft: Zhenyu Peng
Writing – review & editing: Zhenyu Peng, Xin Wang, Fabien Graveleau, Bruno C. Vendeville

Abstract In the rejuvenated mountain front, preexisting basement structures are often reactivated and interact with the subsequent thin-skinned deformation. How the deep structures affect the shallower ones is key to establishing the processes and mechanisms for the foreland fold-and-thrust system. We presented an exceptional case study on the structural inheritance between the deep Mesozoic strike-slip faults and the shallow Cenozoic contractional folds from the Northern Tianshan foreland basin, Northwest China, using high-resolution 2-D and 3-D seismic data. Based on the interpretation of seismic data and progressive restoration, our study illustrated the NW-trending Ai-Ka strike-slip faults controlled a dextral shear zone, which initiated the Gaoquan restraining bend in the basement during Jurassic. Later, these strike-slip structures, close to the mountain front, were reactivated during the N-S Mio-Pliocene contraction, and folded the upper *décollements* that characterized the localization of thin-skinned deformation. In contrast, in the further foreland, nonreactive strike-slip faults controlled basal *décollement* pinch-out, which localizes the thin-skinned deformation, resulting in *en échelon* folds that trace the strike of the deep strike-slip faults. The onset time of each anticline shows that the thin-skinned deformation first extended laterally and then propagated further north, resulting in ca. 7 km shortening along the whole foreland. Moreover, the shortening rate decreased eastward from 0.90 to 1.46 mm/yr along the Gaoquan-Kayindike structural line to 0.24–0.37 mm/yr along the Dunan structural line as the Sikeshu depression, constrained by the NW-trending Ai-Ka strike-slip fault, narrowed eastward. This feature implies that the width of the depression may control the amount of displacement propagation.

1. Introduction

The role of preexisting structures or heterogeneities in controlling subsequent deformation has long been a well-known issue (Bonini et al., 2015; Butler, 1989, 2017; Butler et al., 2006; Cooper et al., 1989; Granado et al., 2018; Laurent et al., 2021; Ravaglia et al., 2006; Williams et al., 1989). Reactivated structures have been discovered at the mountain piedmont of many fold-and-thrust belts (FTBs), such as in the Alps (Philippe et al., 1998), Andes (Carrera & Muñoz, 2013; Giambiagi et al., 2008), Sevier (Miller, 2003), Jura (Madritsch et al., 2008), Pyrenees (Carola et al., 2013), Zagros (Molinaro et al., 2005; Mouthereau & Lacombe, 2006; Mouthereau et al., 2007), and Variscan Mountains (Krzywiec et al., 2017). Traditionally two end members in the deformation style of FTBs are distinguished: thin-skinned versus thick-skinned deformation (e.g., Lacombe & Bellahsen, 2016; Pfiffner, 2017). Thin-skinned deformation refers to the development of thrust sheets where the sedimentary cover is detached from its crystalline substratum along a *décollement* layer that generally consists of mechanically weak rocks, for instance, evaporites or over-pressurized clays (Chapple, 1978; D. M. Davis & Engelder, 1985). In contrast, thick-skinned deformation involves crystalline basement faults that root in deep crustal weakness located in the middle or lower crust (Pfiffner, 2017). Thick-skinned structures are more likely to be reactivated in subsequent tectonic systems (Madritsch et al., 2008). The preexisting basement structures are considered weak zones that could concentrate strains as they are transmitted in the continental crust ahead of the growing mountain belt (Butler, 2017; Laurent et al., 2021; Tavarnelli et al., 2004).

Structural inheritance is therefore one of the fundamental factors that affect the diversity of FTBs by changing the rheology of the basement rocks in foreland basins (Butler, 1989). For this reason, the interaction between the inherited structures and the subsequent tectonic deformation triggers a large variety of structures in FTBs globally, including normal fault reactivated by crustal shortening (positive inversion tectonics), thrust fault reactivated

during extension (negative inversion tectonics), interactions between strike-slip faults and the younger thrusts or normal faults, and so on (Bonini et al., 2015; Butler, 1989; Butler et al., 2006; Hessami et al., 2001; Homberg et al., 2002; Tavarnelli et al., 2004; Windhoffer et al., 2005). The mechanical influences of structural inheritance on the pattern of FTBs have also been investigated extensively by analog and numerical modeling approaches (Bonini et al., 2015; Granado & Ruh, 2019; Ruh & Vergés, 2018; Schori et al., 2021; Selander et al., 2012; Windhoffer et al., 2005). Nevertheless, how preexisting strike-slip faults affect the structural pattern and deformation history of subsequent FTBs in foreland basins remain elusive. One approach to reveal their structural geometry is via the interpretation of high-resolution seismic data. Moreover, 3-D seismic data is optimal for studying the reactivation of strike-slip faults, because one can investigate the influences of structural inheritance in both the cross-sectional view and the map view.

This study aimed to document and deepen the understanding of the geometrics, kinematics, and impacts of inherited strike-slip fault zones (or wrench tectonics) on the compressional pattern of a subsequent FTB. To achieve this goal, we chose Northern Tianshan FTB which had undergone thick-skinned shortening and strike-slip deformation in the Mesozoic era (e.g., Allen et al., 1991; Laurent-Charvet et al., 2002; Y. Yu et al., 2016; Zhu et al., 2023) and thin-skinned thrust deformation in the Cenozoic era (Avouac et al., 1993; Burchfiel et al., 1999). Based upon the extensive 2-D and 3-D seismic data acquired during petroleum exploration in this region, we interpreted the geometry and kinematics of the preexisting basement strike-slip faults and subsequent thin-skinned deformation. Using structural modeling and balanced restoration methods, we further quantified the shortening of the cross-sectional and selected individual structures to analyze the geometry of the growth layer and the type of multiphase structural deformation. With these results from Northern Tianshan foreland basin, we attempted to gain new insights into the role of basement strike-slip faults on the shallow contractional structures.

2. Geological Background of the Northern Tianshan Foreland Basin

2.1. Tectonic Setting

The Tianshan Mountains span over 2,400 km in Central Asia (Figure 1a) and have experienced a protracted, multiphase tectonic deformation history since the Paleozoic (e.g., Jolivet, 2017; Windley et al., 2007; Wilhem et al., 2012). During the final accretion of the Tianshan terranes in Permian, the southward subduction of the North Tianshan Ocean (also called the Junggar-Balkash Ocean) underneath the Yili block ended with the collision between the Yili and North Tianshan-Junggar blocks (Jolivet, 2017) which formed a suture zone between the Junggar Basin and the North Tianshan (e.g., Han et al., 2010). This suture zone was later reactivated as a lithospheric-scale strike-slip fault, named Northern Tianshan Fault (NTF), during the Mesozoic (e.g., Morin et al., 2020; Figure 1a).

Since the early Mesozoic, the Tianshan range experienced transpressional deformation in response to the oblique convergence between the Siberia and Baltica cratons (Bazhenov et al., 1999; Van der Voo et al., 2006), which induced dispersed rotations of crustal blocks and motions along the basement strike-slip faults (e.g., Allen et al., 1991; Buslov et al., 2004; Laurent-Charvet et al., 2002; Van der Voo et al., 2006). For example, estimates of the displacements were approximately 1,570 km $\pm$ 280 km along the Irtysh-Gornotsaev shear zone along the southern edge of the Altai Mountains, and 490 $\pm$ 250 km along the NTF (Figure 1a) (Choulet et al., 2011). In addition, basement cooling ages and a widespread regional unconformity at the base of the Cretaceous unit in the northern Tarim and southern Junggar basins indicated renewed tectonic deformation and basin inversion across the Tianshan range during the Late Jurassic (De Grave et al., 2007; Glorie et al., 2010; Vincent & Allen, 2001; Ma et al., 2015; W. Yang et al., 2015; Figure 2). This tectonic deformation may have been driven by the far-field accretion of the Lhasa block along the southern margin of Tibet (Kapp et al., 2007) and the closure of the Mongol-Okhotsk Ocean in Siberia (Zorin, 1999).

Since the Late Oligocene (~23–25 Ma), far-field effects of the India-Eurasia continental collision caused the thick-skinned tectonic reactivation of the Paleozoic and Mesozoic basement structures in Tianshan, which strongly rejuvenated its topography (e.g., Burchfiel et al., 1999; Charreau, Gumiaux, et al., 2009; Dumitru et al., 2001; Glorie & De Grave, 2016; Hendrix et al., 1992; Jolivet et al., 2018; Macaulay et al., 2014; Sobel et al., 2006). Two major phases of uplift and erosion occurred in the Middle Miocene at ~16–15 and ~11–10 Ma (Charreau, Chen, et al., 2009). Adjacent to the northern Tianshan range, a FTB developed as thin-skinned deformation in the southern Junggar Basin, and triggered the 1906 M 7.7 Manas earthquake and the 2016 M 6.2 Hutubi earthquake

10.1029/2023TC007986

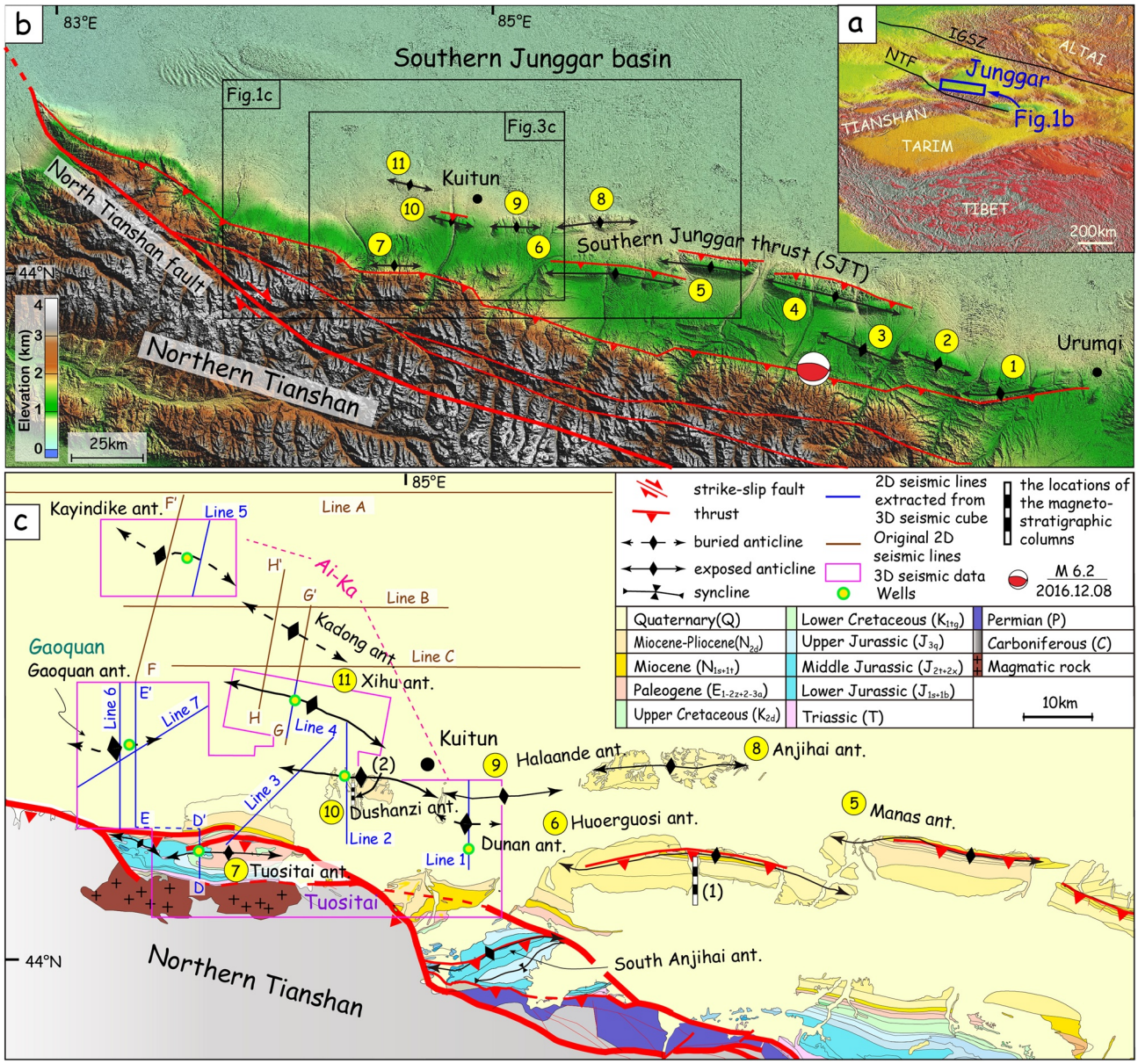

Figure 1. Topographic and geological map of the western part of the Northern Tianshan foreland basin. (a) Location of the Junggar Basin in central Asia. The Junggar Basin is bounded by the Irtysh-Gornotsaev shear zone along the southern edge of the Altai Mountains and the Northern Tianshan Fault along the northern edge of the Tianshan Mountains. (b) SRTM-derived, color-shaded relief map of the Northern Tianshan foreland basin. Three *en échelon* fold belts are exposed in the foreland basin. First row: (1) Kalazha anticline; (2) Changji anticline; (3) Qigu anticline. Second row: (4) Tugulu anticline; (5) Manas anticline; (6) Huoerguosi anticline; (7) Tuositai anticline. Third row: (8) Anjihai anticline; (9) Halaande anticline; (10) Dushanzi anticline; (11) Xihu anticline. The focal mechanism of the 2016 Hutubi earthquake is indicated (R. Q. Lu et al., 2018). (c) Geological map of the western and central parts of the Northern Tianshan foreland basin. Buried structures along the Gaoquan and Ai-Ka structural systems are indicated. Pink polygons and blue lines mark the location of seismic databases (3-D seismic cubes and 2-D lines, respectively) used in this study. The black-white bar represents the location of two magnetostratigraphic sections: (1) Jinggou He section (Charreau, Chen, et al., 2009; Charreau, Gumiaux, et al., 2009), (2) Kuitun He section (Charreau et al., 2005).

(e.g., Avouac et al., 1993; Charreau et al., 2008; Guan et al., 2016; R. Lu et al., 2018; Molnar & Ghose, 2000; Qiu et al., 2019; Stockmeyer et al., 2014).

2.2. Structures

The Northern Tianshan FTB is composed of three major *en échelon* east-trending fold belts (Figure 1b). From south to north, the first row of the folds consists of the Kalazha, Changji, and Qigu anticlines. The second

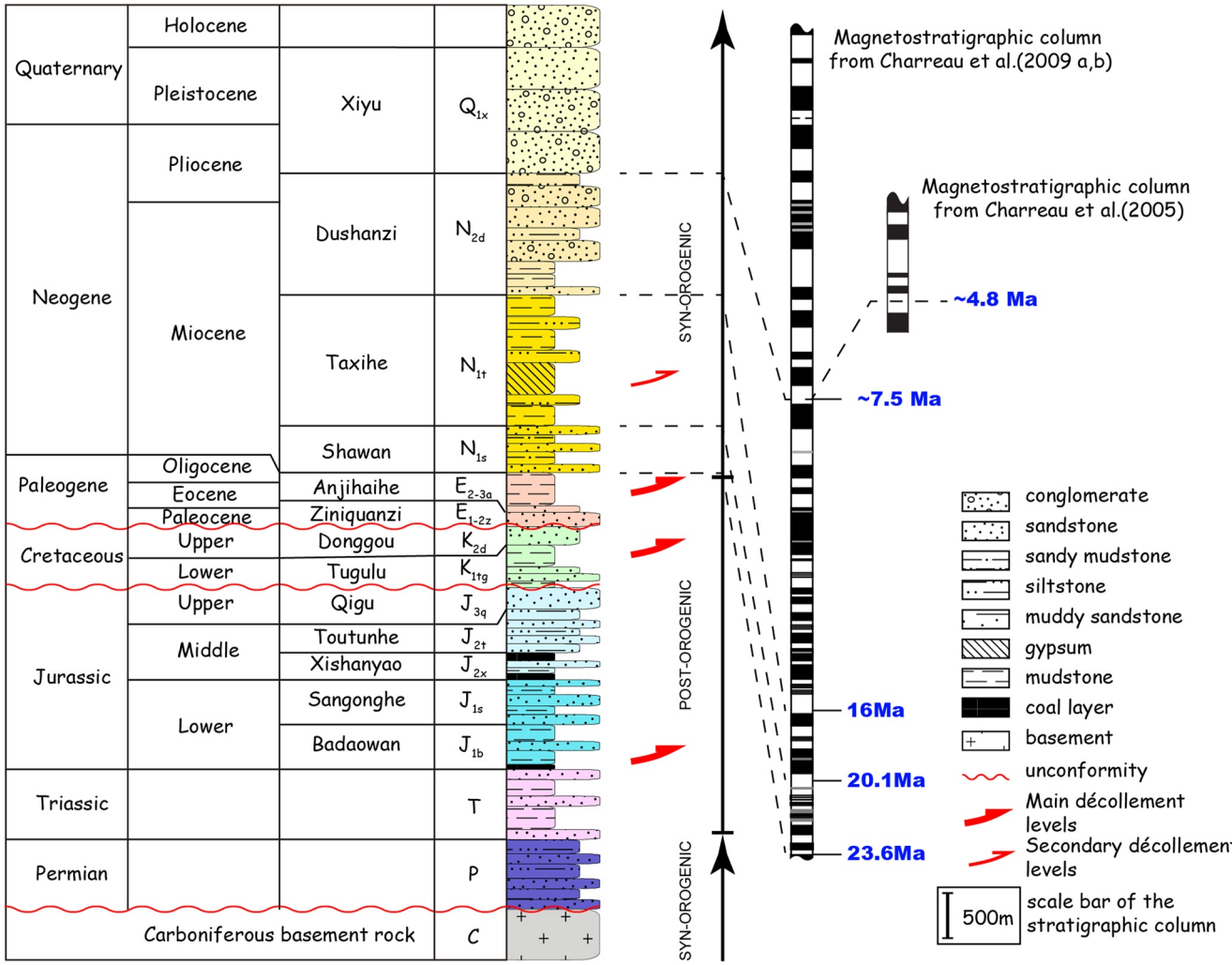

Figure 2. Synthetic lithostratigraphic log of the Northern Tianshan foreland basin. Lithological data from the Xinjiang Oilfield Company of PetroChina (Dong et al., 2017; Gao et al., 2013; Tan et al., 2016; Z. Wang et al., 2009). The geological time is based on the Geologic Time Scale v.6.0 (modified after Walker et al., 2013) and combined with the magnetostratigraphic columns from the Kuitun He section (Charreau et al., 2005) and Jingou He section (Charreau, Gumiaux, et al., 2009; Charreau, Chen, et al., 2009).

row comprises the Huoerguosi, Manas, Tugulu, and Tuositai anticline. The Anjihai, Halaande, Dushanzi, and Xihu anticlines constitute the third row. The activation and growth of these structures and the rise of the present-day topography characterized the Quaternary deformation (e.g., Avouac, 1993; Burchfiel et al., 1999; H. Lu et al., 2019; Molnar et al., 1994; Qiu et al., 2019). The accommodation of shortening and growth of the fault-related anticlines is generally considered to be strongly controlled by three major *décollement* layers in the foreland basin (Figure 2). From top to bottom, they are localized in the Paleogene Anjihaihe Formation ($E_{2\sim3a}$) (e.g., Guan et al., 2016; Qiu et al., 2019; Stockmeyer et al., 2014), Lower Cretaceous mudstone layers in the Tugulu Formation (K_{1tg}) (e.g., Li et al., 2020), and Lower Jurassic Badaowan Formation (J_{1b}) (e.g., F. Yu et al., 2012; Shen et al., 2022). These detachments may not be activated simultaneously in each structure, depending on local variation of stratigraphic facies and/or fluid overpressure conditions, such as the detachment in the Dushanzi anticline (Luo et al., 2007; Wan et al., 2015). In this study, we also offered evidence of another small-scale detachment within the Miocene Taxihe Formation (N_{1t}) in the Gaoquan area.

Recent 3-D seismic surveys in the western part of the Northern Tianshan FTB (Figures 1c and 3) have unraveled and characterized four buried anticlines: Gaoquan, Kayindike, Kadong, and Dunan (Du et al., 2019; Y. Wang et al., 2020; Zhou, 1994). The latter three, together with the Dushanzi and Xihu anticlines, form the Ai-Ka *en échelon* fold system (D. Yang et al., 2019) (Figure 1c). Interestingly, the Gaoquan, Huoerguosi, Manas, and

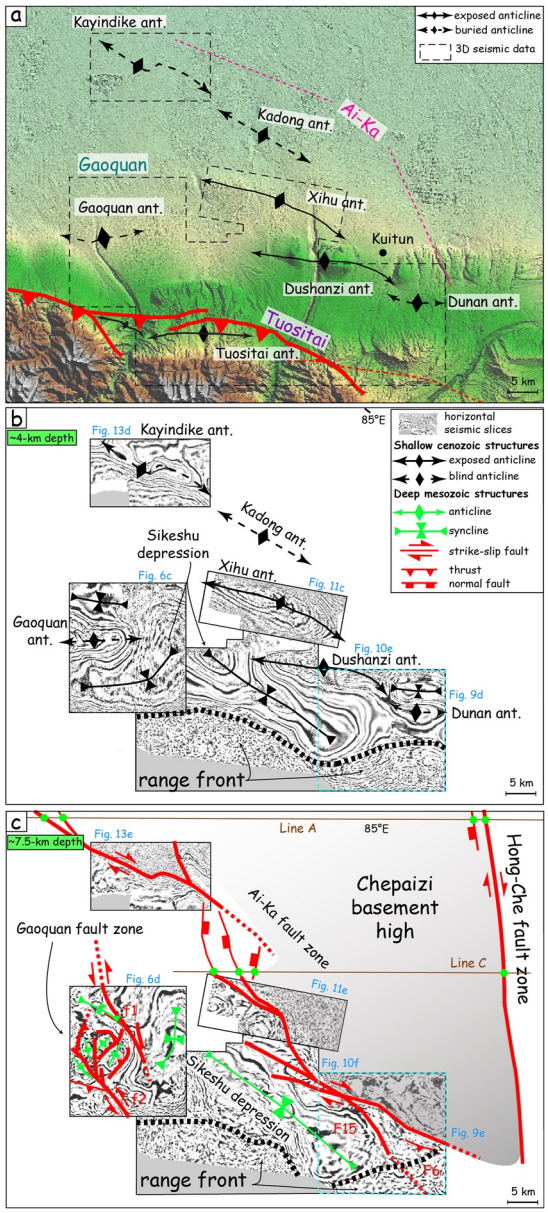

Figure 3. Map-view geometry of the Gaoquan and Ai-Ka structure systems, from the surface to ca. 7.5-km depth. (a) Simplified structural map superimposed on the topographic map of the western part of the Northern Tianshan foreland basin. (b, c) Interpretation of horizontal seismic slices extracted from 3-D seismic data at approximately 4 and 7.5 km depth, respectively, illustrating shallow anticlines and deep strike-slip fault zones. (b) On the shallower seismic slices, the Gaoquan anticline presents E-W strikes, and the Ai-Ka structural systems display five right-stepping *en échelon* anticlines with an overall NW-SE strike. From south to north, these are the Dunan, Dushanzi, Xihu, Kadong, and Kayindike anticlines. A NW-trending syncline (Sikeshu depression) is located between the Gaoquan and Ai-Ka structure systems. (c) On the deeper seismic slices, two sets of NW-striking strike-slip fault zones emerge in the Gaoquan and Ai-Ka areas. The triangular-shaped Chepaizi basement high is also present, bounded by the Hong-Che and Ai-Ka fault zones. Green dots along lines A and C refer to the positions of basement faults identified in the 2-D regional seismic lines (Figure 4).

Anjihai anticlines display an east-trending axis, whereas the Ai-Ka structural system, overall, strikes NW-SE. The reason for this difference is unclear yet and is the subject of this study.

2.3. Stratigraphy

Several thousand meters of nonmarine sedimentary deposits accumulated in the Northern Tianshan piedmont between the Triassic and the Quaternary (Allen and Natal'in, 1995; Hendrix et al., 1992). The Triassic unit comprises alluvial fan and alluvial plain deposits, primarily composed of sandstones and red-to-brown siltstones (Figure 2). The presence of caliche beds indicates deposition in semiarid-to-arid continental conditions (Hendrix et al., 1992; Novikov, 2013). Substantial Lower-to-Middle Jurassic coal deposits and lacustrine/meander belt facies in the Junggar Basin further suggest low-relief depositional landscapes with limited detrital input into the basins (Hendrix et al., 1992). The Lower Cretaceous Tugulu Formation (K_{1t}) sediments are in part lacustrine, comprising a sequence of laterally continuous siltstone and mudstone. The Upper Cretaceous Donggou Formation (K_{2d}) consists of sandy alluvial conglomerate (Hendrix et al., 1992; Figure 2). The Eocene Anjihaihe Formation (E_{2-3a}) comprises shallow lacustrine deposits, composed of mudstone (Gao et al., 2013).

Since Neogene, due to the rejuvenation of the Mesozoic Tianshan orogeny, major uplift and erosion shed large volumes of sediments into the surrounding sedimentary basins, forming the Shawan (N_{1s}), Taxihe(N_{1t}), Dushanzi Formation (N_{2d}) (e.g., Charreau, Chen, et al., 2009) (Figure 2), and the overlying coarse conglomeratic layers of the Xiyu Formation (e.g., Charreau, Gumiaux, et al., 2009; Huang et al., 2010). Magnetostratigraphic studies across the Southern and Northern Tianshan foreland basins have shown that deposition of the base of the Xiyu conglomerates varies by several million years (e.g., Charreau, Gumiaux, et al., 2009; Huang et al., 2010; Qiao et al., 2016; Sun et al., 2004; Thompson Jobe et al., 2018). In northern Tianshan, it ranges between 7.5 Ma in the Jingou He section (Charreau, Gumiaux, et al., 2009) and 4.8 Ma in the Kuitun He section (Charreau et al., 2005) (Figure 2, and see the location of these two sections on Figure 1c). In southern Tianshan foreland, Xiyu Formation can even be as old as 15 Ma (Heermance et al., 2007). The basal Xiyu conglomerates are therefore a diachronous basal contact, extending from the late Neogene to the Quaternary (e.g., Huang et al., 2010). In our study, we used these magnetostratigraphic studies to constrain the age of Cenozoic beddings on seismic lines and therefore to document the growth history of structures.

3. Data and Methods

This study used 3-D and 2-D seismic reflection data, wells and geological map. The seismic datasets were obtained by the Xinjiang Oilfield Company, PetroChina, during oil and gas explorations. The 3-D seismic data were acquired in 2019 and covered an area of 2,450 km^2. They were divided into 4 surveys (Gaoquan, Xihu, Tuositai-Dushanzi, and Kayindike). The 2-D seismic lines were produced in 2011 and had been used to cross-check interpretations of the 3-D seismic data and to fill in the imaging gap between seismic cubes (see the locations in Figure 1c). The vertical resolution of these seismic reflection data is about 25 m. The original 2-D seismic profile and the Tuositai-Dushanzi, Kayindike 3-D seismic data were produced in time. Gaoquan and Xihu 3-D seismic data were produced in depth.

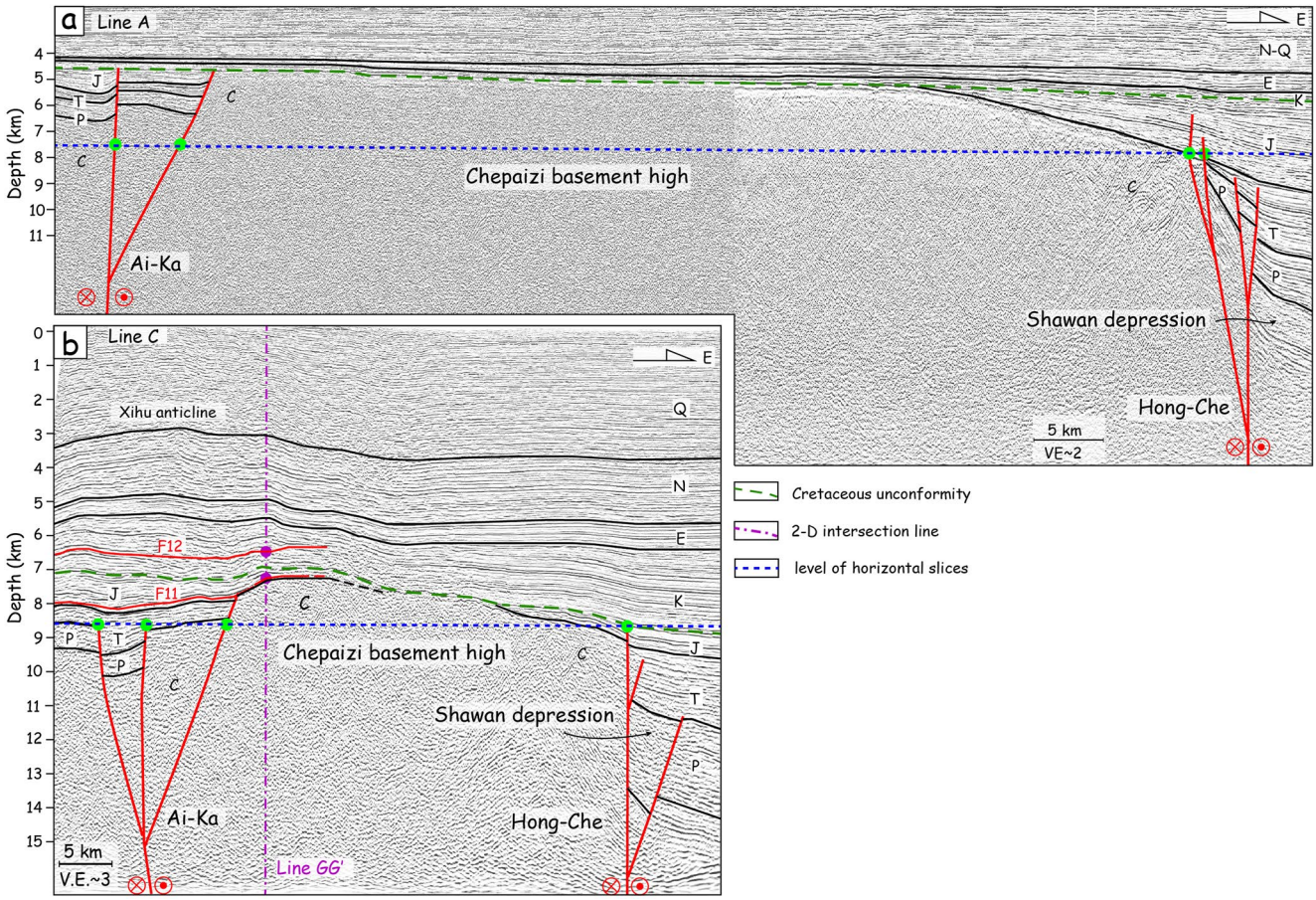

Figure 4. Cross-sectional geometry of the Chepaizi Basement High (CBH) and the Ai-Ka and Hong-Che fault zones, interpreted on seismic lines A and C (see Figures 1c and 3c for their locations). (a, b) The CBH is surrounded by the Permian to Jurassic basin fill on its western side and the Shawan depression on the eastern side. The limit is marked by negative flower structures along the Ai-Ka and Hong-Che fault zones, respectively. The width of the CBH decreases southward (from line A to line C), illustrating a triangular geometry in map view (Figure 3c). The CBH is covered by the regional Cretaceous unconformity (green dashed line), which is barely deformed to the north (line A) but folded to the south (line C).

We converted time sections in depth by using StructureSolver© software, see Figure S7 in Supporting Information S1 and reference video (https://www.structuresolver.com/video-gallery/using-structuresolver-basics/calibrating for the process). For the depth-conversion, we set an average velocity model (3,500 m/s) referred to sonic logs in the region. While conducting depth-conversion, uncertainties arose from the average velocity model which leads to a reduced vertical exaggeration of deep structures, specifically those below 4 s in Two-Way-Travel time (T.W.T). This was because, the sonic log showed a higher velocity model ranging from 3,500 to 4,000 m/s below 4 s in T.W.T. However, by using the average velocity model, converted profiles showed accurate ties between well and seismic data and provided reasonable geometries of the structures. All the seismic reflection profiles were adjusted to a common datum and interpreted in depth.

Surface geology was considered by integrating unpublished 1:200,000 geological maps from the Xinjiang Bureau of Geology and Mineral Resources. For buried structures of Gaoquan, Xihu and Kayindike, horizontal depth slices were extracted from the 3-D seismic data set to image the map-view evolution of the structures with depth (Figure 3a–3c).

After completing the depth-conversion, we employed a restoration methodology to quantify the kinematic evolution of major structure and considering some assumptions. First, we assumed that vertical sediment compaction is negligible during structural deformation, which maintained a constant bedding area on the profile. Second, for flower structures observed in the lower parts of the sections, the restoration approach only accounted for vertical motion, while out of plane movement was restricted to horizontal motion, which did not disturb the vertical restoration. Following these assumptions, shortening computed from balanced cross-sections should be considered as

a minimum estimate. If considering the Layer Parallel Shortening/Layer Parallel Compaction (LPC), the uncertainty of restored shortening could be 5%–25% (Butler & Paton, 2010; Craddock and van der Pluijim, 1989; Engelder & Engelder, 1977; Engelder & Geiser, 1979; Henry et al., 2003; Koyi et al., 2004; Nilforoushan et al., 2008; Sans et al., 2003; Weil & Yonkee, 2009; Whitaker & Bartholomew, 1999; Wiltschko et al., 1985).

To interpret the geometry and kinematics of the Neogene thrust-related folds and the pre-Cretaceous strike-slip faults, we adopted two different approaches.

For the Neogene thrust-related folds, we selected the cross-sections that are perpendicular to the crest of anticline. Then, we used the fault-bend fold techniques (e.g., Suppe, 1983; Suppe et al., 2004; Shaw et al., 2005) to produce a quantitative geometric interpretation of the anticlines. We determined the timing of deformation for each anticline by combining it with growth strata analysis (explained in Text S1 in Supporting Information S1) based on the theoretical studies (Medwedeff, 1990; Suppe et al., 1992, 2004) and magnetostratigraphic studies (Charreau et al., 2005; Charreau, Gumiaux, et al., 2009; Charreau, Chen, et al., 2009). We further adopted the restoration and forward modeling techniques using the StructureSolver© software package to validate our interpretation (Eichelberger et al., 2015) (explained in Text S2 in Supporting Information S1 and the user workshop (StructureSolver LLC, 2009–2019, 2022) https://doi.org/10.6084/m9.figshare.20444976.v1). From there, we estimated the amount of thrust displacement.

For the Mesozoic strike-slip faults that are overlain by the major Cretaceous unconformity, we assume the unconformity surface to be initially flat and subsequently deformed. So we set the unconformity as a reference horizon in each seismic data. Then, we restored ("flattened") it in StructureSolver© to reconstruct the underlying structures in the Late Jurassic. We then extracted horizontal slices from the 3-D seismic data to show the pre-Cretaceous fault trace in map view. We also interpreted cross sections perpendicular to the fault's strike to identify the growth strata to constrain the onset time of the strike-slip faulting. Finally, we integrated these pieces of information in a 3-D model to demonstrate the spatial correlation between the pre-Cretaceous and Cenozoic structures.

4. Results

4.1. Structures in the Northern Tianshan Foreland Basin

4.1.1. Shallow Versus Deep Deformation

Two horizontal depth slices at approximately 4 and 7.5 km, respectively, were extracted from the 3-D seismic data that covered the major structures in the Ai-Ka and Gaoquan areas (Figure 3). Our interpretation showed that the map-view structural geometry changed as a function of depth. At ∼4 km depth, the horizontal seismic slices showed the arrangement of several folds (Figure 3b). An E-trending anticline was present in the Gaoquan area. The Ai-Ka structure system consisted of five NW-trending, right-stepping *en échelon* anticlines. From south to north, they were the Dunan, Dushanzi, Xihu, Kadong, and Kayindike anticlines. Fold axes of the Kayindike, Dushanzi, and Dunan anticline all displayed an S-shaped geometry. In contrast, the Kadong and Xihu anticlines' fold axes were more linear. Between the Gaoquan and Ai-Ka structure systems, the Sikeshu depression consisted of two branched synclines. The eastern one strikes NW-SE, whereas the other displayed a curved axis turning from E-W to NE-SW.

Below these shallow anticlines, the ∼7.5 km-depth horizontal slices illustrated a distinct structural style. Two sets of fault strikes can be identified: the NNW-striking Gaoquan fault zone on the western side of the study area, and the NW-striking Ai-Ka fault zone in the central region. In the Gaoquan area, two NNW-striking branch faults (f1 and f2) were relayed by several NE-trending compressive structures (thrusts and anticlines). In contrast, NW- to NNW-striking right stepping fault segments were interpreted along the Ai-Ka fault zone. In addition, between the Xihu and Kadong anticlines, we interpreted N- to NW-striking normal faults (Figure 3c). Along Ai-Ka, the deep fault segments were consistent with the shallow right-stepping *en échelon* folds. At this 7.5 km depth, the NW-trending Sikeshu depression was still detectable, but it was limited by the Ai-Ka fault zone to the east.

On the eastern side of the study area, a large domain characterized by chaotic seismic facies corresponds to the Chepaizi Basement High (CBH), which was composed mainly of Carboniferous basement rock (Z. Chen et al., 2016). The NW-striking Ai-Ka fault zone represented the structural boundary between the CBH to the east and the Sikeshu depression to the west. We analyzed the CBH features in the next section. To the east, the Hong-Che fault zone limited the CBH to the Shawan basin.

4.1.2. Chepaizi Basement High and Its Bounding Faults

We used several E-W-oriented regional 2-D seismic lines to characterize the CBH, but here we only showed two of them: lines A and C. The CBH showed chaotic seismic facies in the central domain, and its bounding faults (Ai-Ka to the west, and Hong-Che to the east) characterized the surrounding basins (Figure 4). The CBH dipped and narrowed southward at the same time. In profile A, the burial depth of the CBH was approximately 4.5 km and its width was 70 km, while in profile C, the burial depth was about 7 km and the width was only 38 km (Figures 4a and 4b). We found that the top surface of CBH dipped southward and that its W-E width also decreased toward south.

Along the boundaries of the CBH, the Ai-Ka, and Hong-Che fault zones manifested as negative flower structures. Upon analyzing the kinematics of these faults on the basin side, we noted a consistent feature: both zones exhibited normal fault offsets. Specifically, there was a downward offset of Triassic to Jurassic beddings relative to their counterparts on the opposite side of the fault. There was also a contrary feature between Line A and Line C for the CBH. On Line A, the Cretaceous unconformity that covered the CBH was flat, while on Line C the unconformity was folded. Particularly on the left (western) side of Line C, where the seismic line crossed the forelimb of the Xihu anticline. Furthermore, we tentatively interpreted two detachments F11 and F12 at the forelimb of the Xihu anticline. This was because, above the detachment F12, the Cretaceous-Cenozoic beddings had higher amplitude than that below the level of detachment F12 (Figure 4b). Our seismic interpretations on the other seismic profile (Line GG') in perpendicular direction supported the existence of these two *décollements* (F11 and F12) (refer to Figure 11). The purple dashed line illustrated the intersection point between Line C and Line GG' (see Figure 1c for the location).

4.1.3. Cross-Section of the Study Area

We computed a regional synthetic N-S seismic profile DF' to document the structural evolution of deep flower structures and the overlying compressional structures, and to propose a structural interpretation of the Northern Tianshan foreland basin (Figure 5). This profile was composed of three adjacent segments. D-D' and E-E' were extracted from the 3-D seismic data, and Line FF' was an original 2-D seismic line (Figure 1c). This synthetic seismic line intersected three major structures which were, from south to north, the Tuositai thrust nappe, the Gaoquan fault system, and the frontal Kayindike structure (in Ai-Ka fault system). Well data at the crest of Tuositai, Gaoquan and Kayindike anticlines were tied to the seismic data, which helps to map horizons. Additionally, surface geology was integrated to relate to structures at depth at Tuositai anticline (Figure 5a).

To the south, at the piedmont of the Tianshan, we interpreted the Tuositai system as an imbricate structure that was composed of three faults: F1, F2, and F3 (Figure 5b-1). The two deep thrusts propagated within two subhorizontal *décollements* layer along (a) the mudstone layer of the Eocene-Oligocene Anjihaihe Formation ($E_{2\text{-}3a}$) for F3 and (b) the gypsum layer of the Miocene Taxihe Formation (N_{1t}) for F2. The Gaoquan anticline was interpreted as an intercutaneous wedge (triangular structure) (K. R. McClay, 1992) that accommodated S-N shortening along the two detachments. The frontal fault-bend fold Kayindike anticline consumed slip along the detachment F4, which was settled in the coal layer of the Jurassic Badaowan Formation (J_{1b}).

At depths greater than 7 km, we interpreted positive flower structures in the pre-Cretaceous basement below the Gaoquan and Kayindike anticlines (Figure 5b-1). These flower structures cut off Carboniferous rocks, Triassic, and Jurassic beddings and were truncated by the Cretaceous unconformity.

4.1.4. Growth Strata

We analyzed growth strata (light yellow in Figure 5b-1) above the thrust-related folds to decipher the first-order kinematics and growth age of each fold. On the forelimb of the Tuositai thrust nappe, the growth strata dated from the Dushanzi Formation (N_{2d}) to Quaternary strata, which suggested that F1, F2, and F3 had been active since the late Miocene to Plio-Quaternary. In the Gaoquan anticline, the fan-shaped growth strata were composed of the Xiyu Formation (Q_{1x}). As the basal age of the Xiyu Formation varied from 4.8 to 7.5 Ma in the study area (Charreau et al., 2005; Charreau, Gumiaux, et al., 2009), we inferred that F3 and F2 were active during the Middle Pliocene and have continued to be active up to the present time. In the Ai-Ka structural belt, the growth strata suggested that detachment F4 was active only during the Late Quaternary, forming the Kayindike anticline. Overall, the timing and location of these thrusts exhibited a first-order "in-sequence" propagation of deformation toward the foreland.

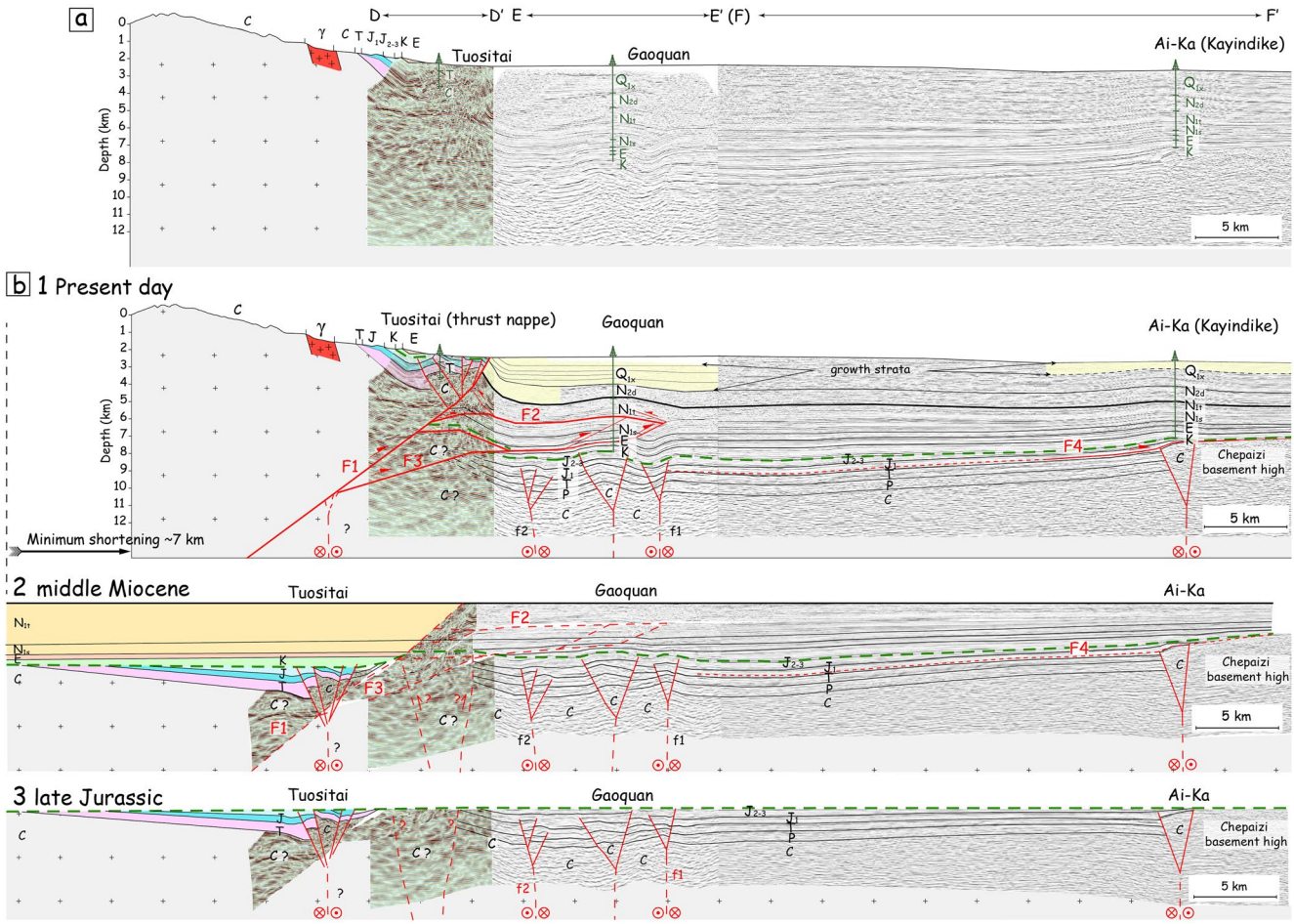

Figure 5. Cross-sectional overview of the structural geometry and the kinematic evolution in the western part of the Northern Tianshan foreland basin, illustrated by the interpretation of the S-N synthetic profiles D-F' (see Figure 1c for locations). (a) Uninterpreted cross section. (b) Interpreted sections. Note that profile DF' is composed of three adjacent lines (3-D seismic cube slice D-D', E-E', and regional 2-D seismic FF'). (b-1) Interpreted regional section illustrating the structural outline of the Tuositai thrust nappe, Gaoquan fold, and Ai-Ka systems (i.e., Kayindike anticline) at present. Three fault styles are present in the section: low-angle thrusts (F1 and F3), shallow detachment faults (F2 and F4), and deep, high-angle faults that form flower structures. (b-2) Section restored to the Middle Miocene stage by flattening the base of the Dushanzi Formation (N_{2d}). The thrust nappe in Tuositai is interpreted as a positive flower structure covered by Cretaceous-middle Miocene strata that have been truncated by F1. Structural restoration yields approximately 7 km of minimum bulk shortening accommodated by the F1 to F4 thrusts since the Middle Miocene. (b-3) Section restored to the Late Jurassic by flattening the Cretaceous unconformity. The restored section shows three deep flower structures in the Tuositai, Gaoquan, and Ai-Ka areas.

4.1.5. Restoration of the Cross-Section

We performed a progressive restoration of the regional cross-section Line DF' using StructureSolver© software (Eichelberger et al., 2015) to quantify its kinematic evolution. By unfolding the base of the Dushanzi Formation (N_{2d}) and the Cretaceous unconformity as the reference horizon, we were able to eliminate deformation caused by the three deep thrusts (F1, F2, and F3). This allowed us to visualize the structural geometry before the deposition of the Dushanzi Formation (ca. 16 Ma) and before the deformation of Cretaceous unconformity (Figures 5b-2 and 5b-3).

By unfolding the base of the Dushanzi Formation (N_{2d}), our restoration showed that thrusts F1, F2, and F3 all rooted at depth in the basement of northern Tianshan hinterland. As they propagated northward, they flattened and branched onto the horizontal Anjihaihe ($E_{2\text{-}3a}$) and Taxihe (N_{1t}) *décollement* layers. Furthermore, the restored Tuositai thrust nappe comprised a positive flower structure that could be tentatively located 7 ± 1.75 km southward of its present-day position and was buried below Cretaceous-Middle Miocene sediments. At that stage, the bedding above the Cretaceous unconformity was already deformed in the Gaoquan area. This implied that the underlying steeply dipping faults were active during the Early-Middle Miocene.

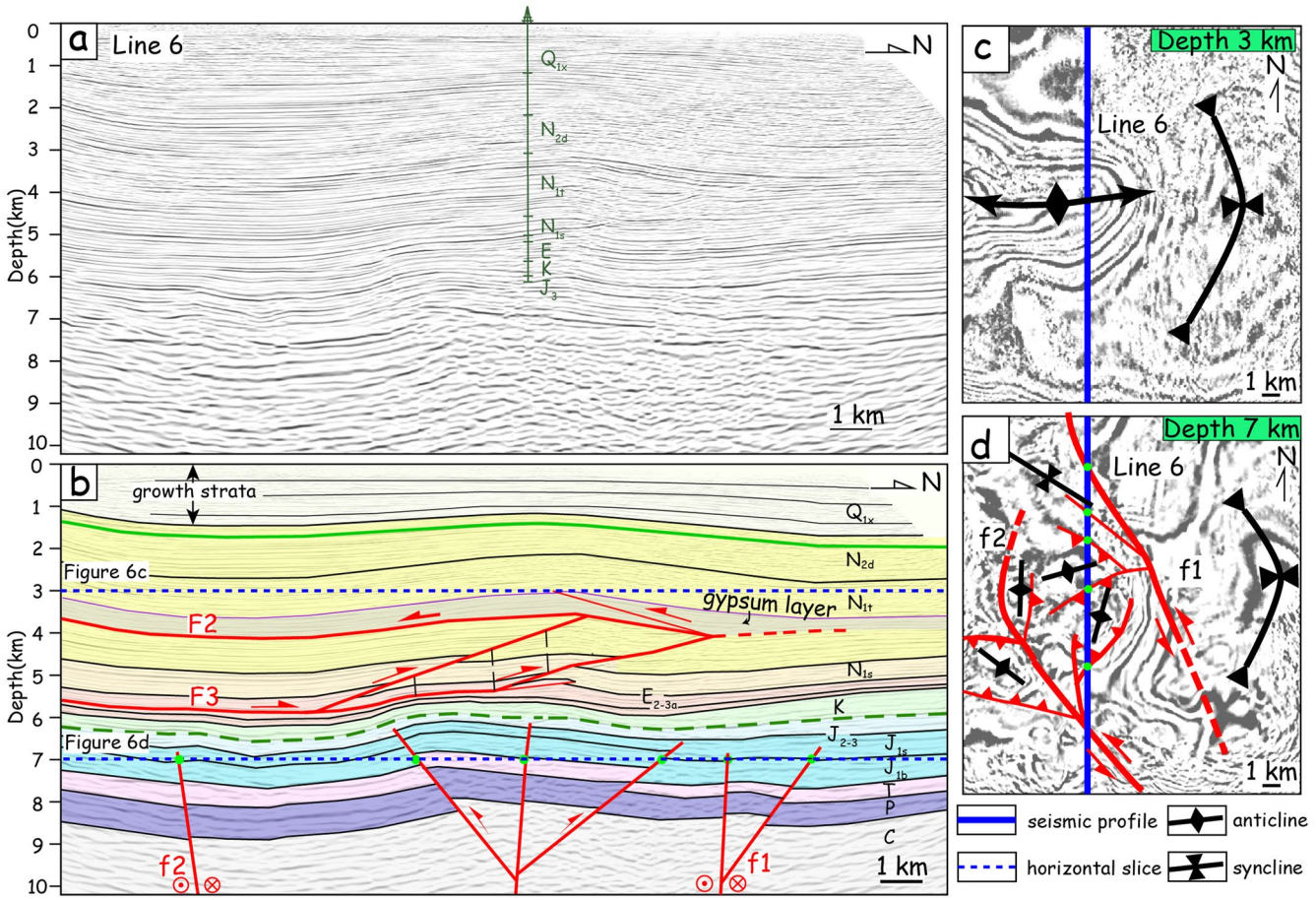

Figure 6. Structural analysis of the Gaoquan anticline. (a) Uninterpreted and (b) interpreted N-S 2-D seismic line 6 (see Figure 1c for locations). Two types of faults are present, including a pop-up/flower structure in the Paleozoic to Mesozoic strata and detachment faults F2 and F3 that form a triangle zone in the overlying Tertiary strata. The shallower detachment F2 is localized along the gypsum layer of the Miocene Taxihe Formation (N_{1t}), and the deeper detachment F3 is rooted in the Eocene-Oligocene Anjihaihe Formation (E_{2-3a}). The level of the horizontal seismic slices is represented by blue dashed line in (b). (c) Shallow (3 km) horizontal seismic slice through the 3-D seismic data, showing an *E*-trending fold axis trace in map view. (d) Deep (7 km) horizontal slice with interpretations, showing two NW-striking fault traces (f1 and f2), and thrust faults in between.

In the second step, we unfolded the Cretaceous unconformity to restore the section in the Late Jurassic (Figure 5b-3). This restoration barely changed the geometry of the underlying flower structures in the Tuositai, Gaoquan, and Kayindike areas. These flower structures offset the Triassic and Jurassic strata, indicating that the western FTB had already experienced deformation before the Cretaceous.

4.2. Gaoquan Structure

4.2.1. 2-D Seismic Interpretation

The Gaoquan anticline is a buried structure located approximately 12.5 km north of the Tianshan mountain front (Figure 3a). We interpreted the 3-D seismic data and present one representative seismic line (Line 6) across the eastern end of the Gaoquan structure (Figure 1c). Two different types of faults were superimposed vertically. Below the Cretaceous unconformity (green dashed line), steeply dipping faults composed a pop-up that affects the Paleozoic, Triassic, and Jurassic strata. Above, low-angle thrusts detached along the mudstone layer in the Eocene-Oligocene Anjihaihe Formation (E_{2-3a}) for F3 and the gypsum layer in the Miocene Taxihe Formation (N_{1t}) for F2 (Figure 6b).

Between the two *décollements* F2 and F3, a small-scale triangle zone interpreted on the seismic profile was characterized by two north-verging ramps that were rooted in the deep *décollement* F3 and branched upward into the upper *décollement* F2. There was also a minor south-verging back thrust rooted in the F2 *décollement*.

The activity of this triangle zone was recorded by the fan-shaped geometry of Pliocene-Quaternary growth strata (Figure 6b). In map view, the fold triggered by this triangular zone trended W-E (Figure 6c).

Below the Cretaceous unconformity, the Mesozoic basement faults cannot be clearly imaged due to the poor quality of the seismic data. However, their location and dip can be inferred from the offsets of the Jurassic and Triassic series. The dip of the deep faults was 45° for some and nearly vertical for others (Figure 6b). We mapped the trace of these faults on the horizontal slice located at approximately 7 km depth (Figure 6d). The result showed two NW-SE right-stepping master faults (f1 and f2), along with reverse faults and small anticlines in between, which composed a restraining bend.

4.2.2. Structural Restoration

We restored seismic Line 6 to decipher the kinematic history of the Gaoquan structure (Figure 7). Our results illustrated three stages: Early Pliocene, Early Miocene and Late Jurassic. Each stage includes (a) a restored 2-D vertical synthetic seismic profile (left column on Figure 7) and (b) a restored horizontal seismic slice computed from the 3-D seismic data (central column on Figure 7). We also included present day structural maps (right column on Figure 7) of some selected horizons (levels H1, H2, H3, and H4 on Figure 7a-1). The seismic profile aimed at illustrating the geometry of structures and identifying the growth strata at each stage. The restored horizontal seismic slice presented the map view geometry of the structure at each restored step. Correlated with the 2-D vertical synthetic seismic profile, the restored horizontal slices provided a 3-D perspective of the Gaoquan structural system. Compared with the present day structural maps at different selected depths (H1–H4), the restored horizontal slices showed the variation of structural high's geometry, amplitude and location through time.

At the present stage (Figure 7a-1), the seismic section corresponded to a simplified version of the interpretation in Figure 6b. A 3-km-deep seismic slice illustrated the E-W trending shallow fold (Figure 7a-2). Then, continuing the restoration, we unfolded the base of the Pliocene-Quaternary growth strata (Figure 7a-1), and reconstructed the structural geometry of Gaoquan anticline at Early Pliocene times (Figure 7b). The restoration quantified a 1 ± 0.25 km shortening for the development of the triangle zone that composed the shallow Gaoquan anticline along *décollements* F2 and F3 (Figures 7a-1 and 7b-1). Although the deformation in Quaternary had been removed, Cretaceous-Lower Miocene beddings were still folded, such as the top surface of Cretaceous (orange horizon) (Figure 7b-1). This fold shape suggested that the basement fault was active before or during the deposition of the Taxihe and Dushanzi Formations (Middle Miocene-Early Pliocene). We attribute this activity to a steep fault f4 in the center of the deep pop-up. In addition, the horizontal slice at 5.5-km-depth crossing the Cretaceous strata illustrated this fold as a round-shaped structural high in the central domain (Figure 7b-2).

Then, we unfolded the top surface of Lower Miocene (yellow level in Figure 7c-1). The restoration result showed a constant thickness interval in Middle Miocene strata, that covered the Gaoquan anticline. This suggested a short quiescence phase with little or no structural relief growth during Middle Miocene. Below this constant thickness interval, the Cretaceous beddings were still folded. This implied that the basement pop-up structure was active from the Eocene to the Early Miocene times, presumably due to the activity of the southernmost fault f5 in the deep pop-up. Also, the horizontal slice at 5.5-km depth still illustrated a round-shaped structural high for this fold (Figure 7c-2).

Finally, we unfolded the Cretaceous unconformity (Figure 7d-1). The steep basement faults f3 and f5 produced a pop-up whose reverse fault kinematics was evidenced by the normal offset of the Triassic to Lower Jurassic beddings. Then sealed by Late Jurassic beddings. These features illustrated that the subvertical reverse faults were active during the Jurassic times. Furthermore, the restored horizontal seismic slice at 6.5-km depth revealed a basement restraining bend limited by two NW-SE fault traces (f1 and f2) (Figure 7d-2).

Comparing all the restored horizontal slices and present day structural maps, we summarized the reactivation process of the basement restraining bend as follow. After the apron-shaped restraining bend deformed at Late Jurassic (Figure 7d-2), an isolated subcircular mole occurred at the same position of the bend in Cretaceous beddings by the Early Pliocene time (Figures 7b-2 and 7c-2). Moreover, on the present day structural maps at horizon H2 and H3, the position and shape of this round-shaped mole were still preserved and has approximately 500–600 m amplitude (Figures 7b-3 and 7c-3). This spatial correlation of the basement restraining bend and overlying isolated structural high at different geological time indicated that from the Jurassic to the Pliocene a thick-skinned deformation controlled the reactivation of the basement restraining bend. Notably, the *décollement* layer in the Eocene-Oligocene Anjihaihe Formation (E_{2-3a}) had been deformed (folded) by the thick-skinned

10.1029/2023TC007986

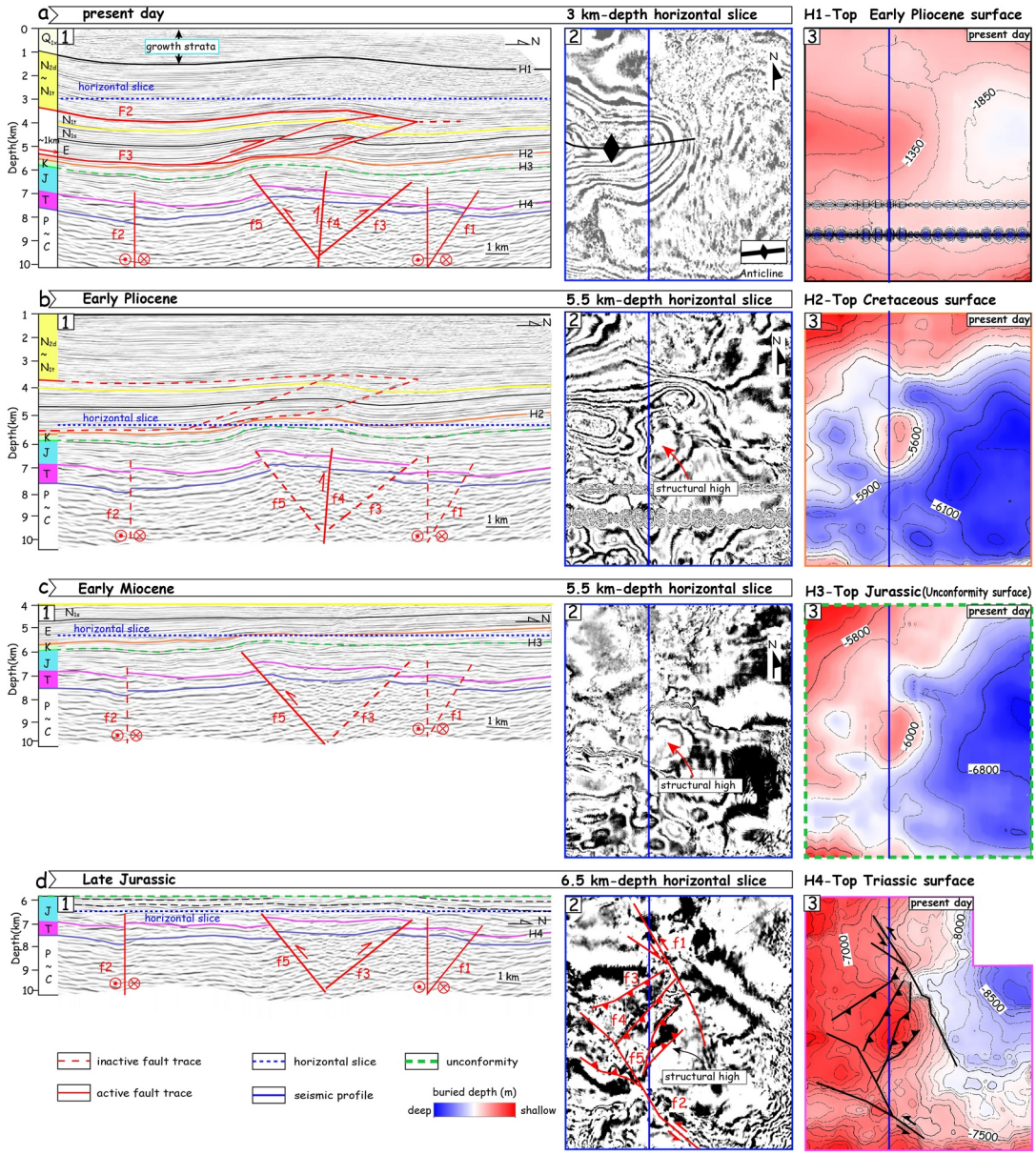

Figure 7. Restoration sequence and structural maps of the Gaoquan anticline and the underlying structures, from the present to the Late Jurassic. The 2-D seismic profile (line 6) and three horizontal seismic slices at 3, 5.5, and 6.5 km depths from the 3-D seismic data are sequentially restored. (a-1) Original seismic profile at present. (a-2) 3 km-depth seismic slice and (a-3) structural map of the top surface of Early Pliocene. The shallow E-W Gaoquan anticline is highlighted. (b-1) Restored seismic profile at Early Pliocene times. The deep, steeply dipping fault zone is reactivated as a thick-skinned structure. (b-2) Seismic slice at 5.5 km depth, showing a round-shaped structural high in the central part at Early Pliocene times. (b-3) Structural map of horizon *E* at present. (c-1) Restored seismic profile at Early Miocene times. The deep steeply dipping fault zone is reactivated as a thick-skinned structure. (c-2) Seismic slice at 5.5 km depth, showing a round structural high during the Early Miocene times. (c-3) Structural map of the top surface of Cretaceous at present. (d-1) Restored seismic profile at the Late Jurassic. The deep steeply dipping fault zone offset strata from the Triassic to Jurassic. (d-2) Seismic slice at 6.5 km depth, showing a set of NW-SE fault traces at the Late Jurassic. (d-3) Structural map of the top surface of Triassic at present. The northwest part of this map was a basement high that was bounded by the NW-SE fault trace.

deformation during Early Miocene (Figure 7c-1). This detachment later transferred a thin-skinned deformation during Quaternary (Figures 7a,1, 7a,2, and 7a-3). However, from the Pliocene to the present stage, whether the thick-skinned structure is still active is unclear. Based on this summary, the local round-shaped basement high at present (Figures 7b-3 and 7c-3) was most likely an inherited structure from the Jurassic-age restraining bend.

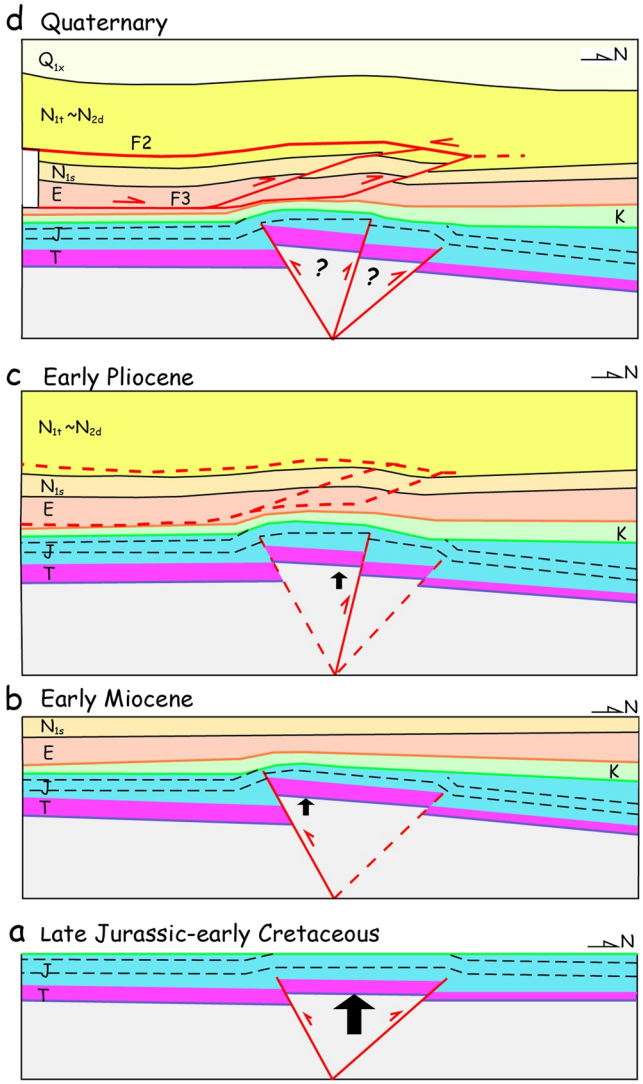

Figure 8. 2-D simplified sketch of the kinematic evolution between the pop-up/flower structure and the shallower thrust-related fold. (a) Initial stage between the Late Jurassic and the Early Cretaceous. The positive flower structure deformed the Triassic-Jurassic strata and ending with a Cretaceous unconformity. (b) The deep, positive flower structure was reactivated as a thick-skinned structure during Eocene time, followed by a stage of tectonic quiescence in Early Miocene time. (c) During Early Pliocene, the thick-skinned structure active again. (d) Since the Quaternary, a thrust wedge forms as a thin-skinned structure and remains active.

According to this sequential restoration, we simplified the basement restraining bend as a pop-up in 2-D forward modeling and summarized the kinematic evolution of the Gaoquan structural system into three main stages (Figure 8):

1. The pre- Cretaceous strike-slip fault formed a flower structure, which was eroded later and covered unconformably by the Cretaceous (Figure 8a).
2. There was a tectonic quiescence during the Cretaceous and the Paleogene. Then, the basement restraining bend reactivated from Early Miocene to Early Pliocene, resulting in folding of the Cretaceous-Middle Miocene beddings (Figures 8b and 8c).
3. Finally, from the Late Pliocene to present, the low angle thrust faults developed along two interbedded *décollements* (F2 and F3) and created the shallow anticlines of Gaoquan structure (Figure 8d).

4.3. Ai-Ka Structure Belt

Below we further interpreted the geometry and kinematics of the Dunan, Dushanzi, Xihu, Kadong, and Kayindike anticlines that composed the Ai-Ka structural belt.

4.3.1. Dunan Anticline

The Dunan anticline is a buried structure located to the east of the Gaoquan structure and approximately 7 km north of the northern Tianshan range front (Figure 3a). The horizontal slice at 4-km depth indicated that this anticline had an E-W fold axis, located at the boundary of the CBH and Sikeshu depression (Figures 3b, 3c, 9d, and 9e). On the 2-D seismic line (Line 1) extracted from the 3-D seismic data and oriented perpendicular to the fold axis, the shallow Dunan anticline appeared as an open, slightly asymmetric, fold with a wide and gently dipping southern limb and a narrow, steep northern limb (Figure 9a). The fold had been buried by approximately 2.1 km-thick late Pliocene-Quaternary sediments.

We interpreted the Dunan anticline as a shear fault-bend fold (Suppe et al., 2004) because the dip of the back limbs of the fold was less than that of the fault ramp (thrust F7). The thrust F7 rooted southward in the Jurassic Badaowan Formation (J_{1b}). Two branch faults (F5 and F6) broke through the forelimb of the anticline, altering the geometry of this structure. Additionally, a low-relief detachment fold or a pop-up-like structure existed north of the Dunan anticline. This detachment fold rooted within the upper flat of thrust F7 that propagated as a *décollement* into the mudstone beddings of the Cretaceous units. Below the Dunan anticline, a steeply dipping fault (Ai-Ka Fault) separated the Sikeshu depression and the CBH. The depression had accumulated 2-km thick Jurassic sediments. The CBH composed of Paleozoic basement rocks was covered by thin Jurassic sediments, where the upper Jurassic units (J_3) were missing and covered by Cretaceous unconformity.

The kinematic evolution of the Dunan anticline had been illustrated by unfolding the base of the fan shape growth strata. The balanced restoration profile (Figure 9c) illustrated the structural scenario at the Early Pliocene. Above the Cretaceous unconformity, sedimentary layers were basically flat and of constant thickness, indicating little or no tectonic deformation between the Cretaceous and the Pliocene. Below the unconformity, the subvertical basement fault (Ai-Ka Fault) was truncated by the Cretaceous unconformity, indicating that it was a pre-Cretaceous fault.

Upon considering the results of restoration, the deformation evolution of Dunan structure can be split in three stages:

10.1029/2023TC007986

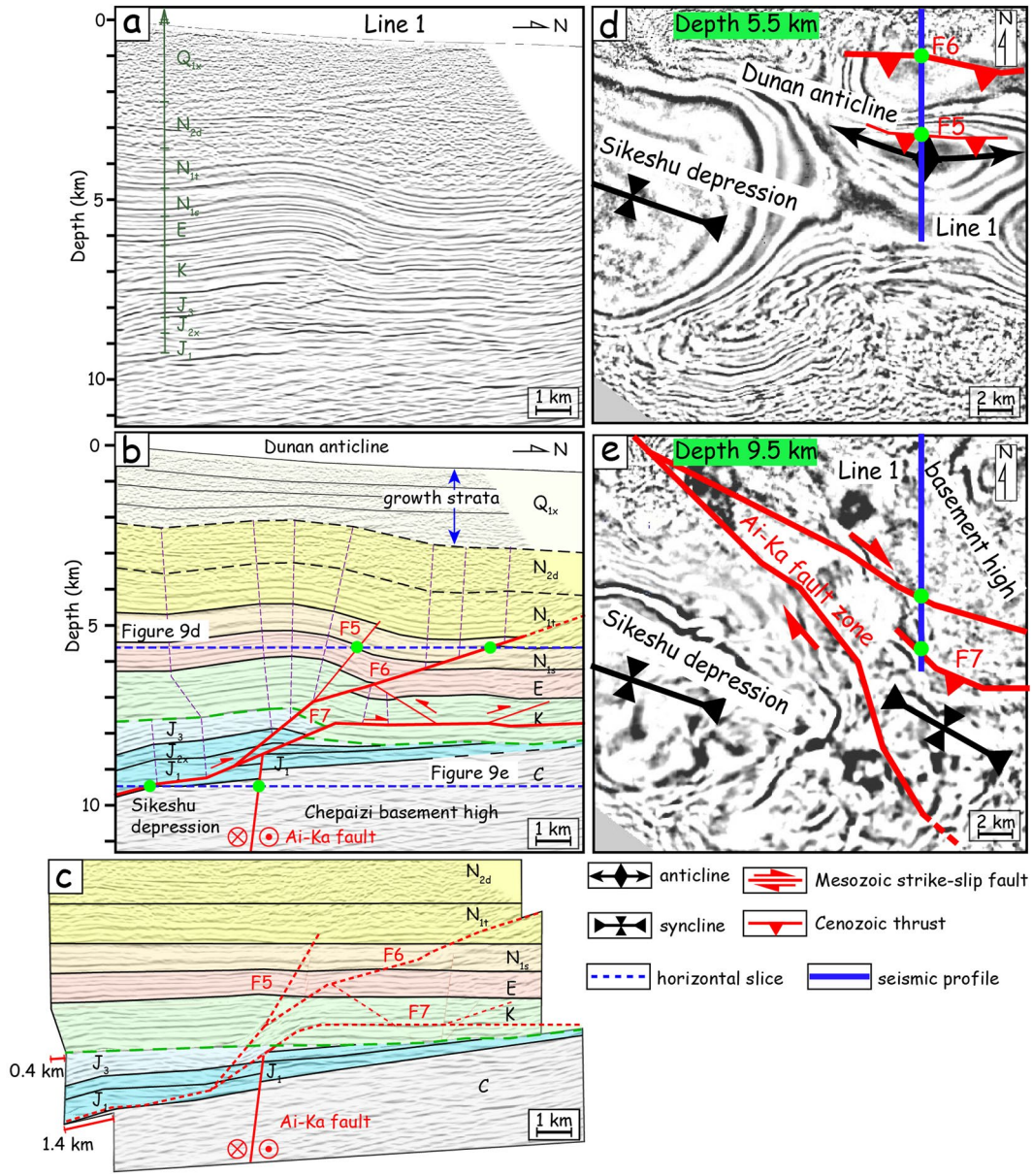

Figure 9. Structural analysis of the Dunan structure. (a) Uninterpreted line 1 extracted from the 3-D seismic data (see Figure 1c for location). (b) Interpreted seismic profile illustrating the Dunan anticline as a fault-bend fold controlled by a basal thrust F6 that has been offset by thrust F5. Below thrust F6, a subvertical fault offsets the Jurassic. (c) Balanced restoration of the Dunan anticline in Pliocene times. Approximately 1.4 ± 0.35 km of shortening has been restored along thrust F6, and approximately 400 ± 100 m of shortening has been restored along thrust F5. Note that the high-angle strike-slip fault trace controlled the thickness variation of Jurassic beddings. (d) Horizontal seismic slice at 5.5 km depth illustrating the fault trace of the *E*-striking thrust F5 and the fold axis of the *E*-trending Dunan anticline. (e) Horizontal seismic slice at 9.5 km depth showing the fault trace of the NW-striking thrust F7 and the Ai-Ka fault zone. These faults separate the Chepaizi basement high (represented by chaotic reflection) to the northeast from the Sikeshu depression (represented by well-imaged reflection) to the southwest.

1. During the Jurassic period, the Ai-Ka Fault was active and controlled the sedimentation of Jurassic unit in the Sikeshu depression.
2. From Cretaceous-Early Pliocene, there was no tectonic deformation in Dunan area, and the Ai-Ka Fault was sealed by thick sediments.
3. From Pliocene to Quaternary, thrust faults and shear fault-bend folds developed. A thrust ramp localized at the former Ai-Ka Fault and accommodated a 1.8 ± 0.45 km S-N shortening.

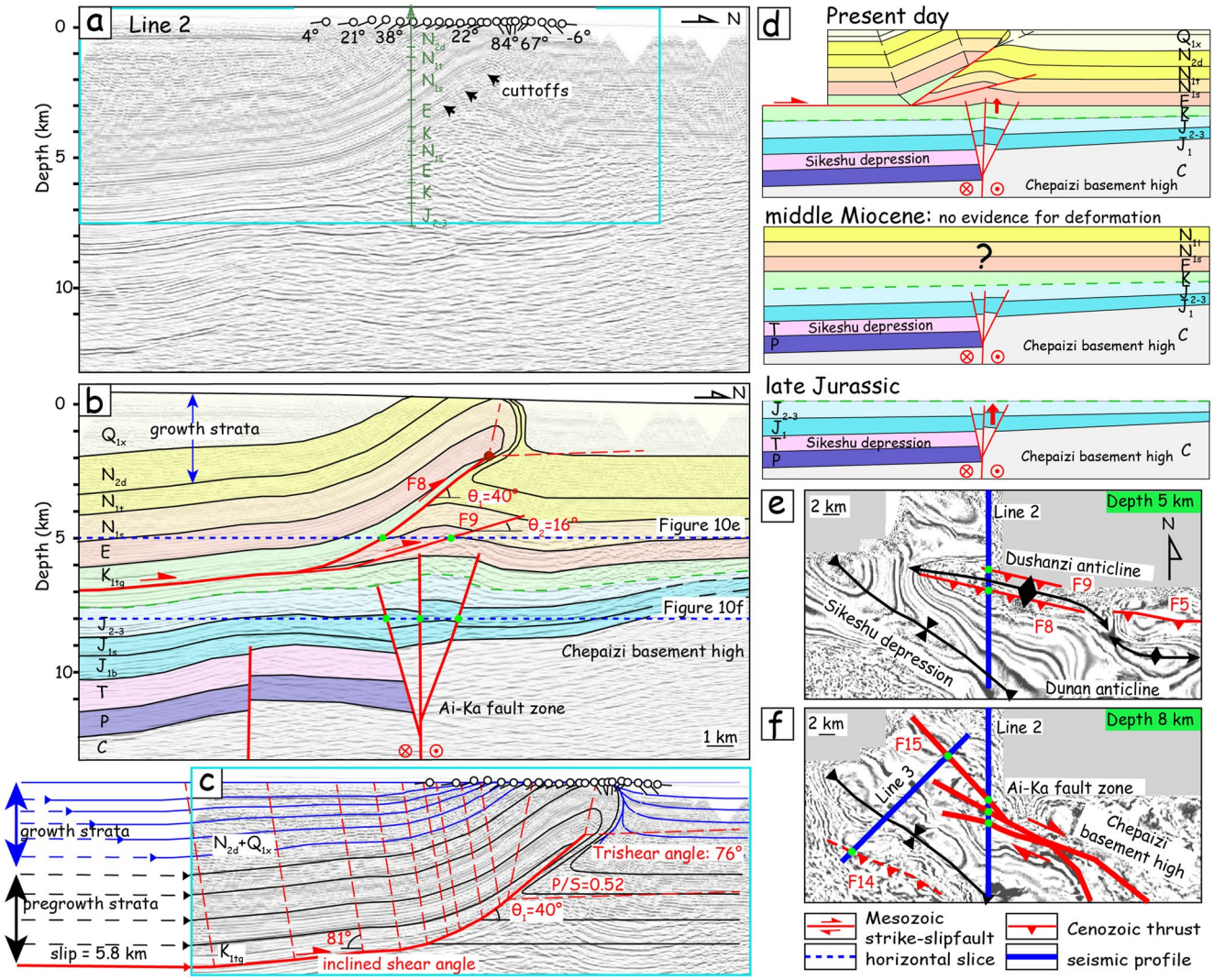

Figure 10. Structural analysis of the Dushanzi anticline. (a) Uninterpreted seismic profile (Line 2) (refer to Figure 1c for locations). The light blue box marks the portion analyzed by forward modeling in (c). The fold shape is asymmetric. The reflector cutoffs indicate the position of a propagating thrust. (b) Interpreted seismic profile illustrating a fault-propagation fold superimposed over a deep flower structure. (c) Best-fit trishear fault-propagation forward model for the shallow Dushanzi anticline and the associated growth strata. (d) Evolution model of the Dushanzi anticline obtained by bed-by-bed restoration. (e) Horizontal seismic slice at 5 km depth, annotated with the traces of Thrusts F5, F8, and F9, and the axes of the Dushanzi and Dunan anticlines. (f) Horizontal seismic slice at 8 km depth, with the interpreted traces of Thrust 14 and the NW-striking Ai-Ka strike-slip fault. These faults separate the Chepaizi basement high (represented by chaotic reflection) from the Sikeshu depression (represented by well-imaged reflection).

A horizontal slice at approximately 5.5 km depth illuminated the shallow anticline and thrusts F5 and F6 (Figure 9d). The slightly curved E-W fold axis was parallel to these two thrust traces, and is perpendicular to the Cenozoic S-N compression. At 9.5 km depth, the horizontal slice intersected with thrust F7, whose trace was parallel to the preexisting Ai-Ka Fault branch (Figure 9e). Furthermore, this preexisting fault separated the CBH (chaotic reflection to the northeast) and the Sikeshu depression (well-imaged reflectors to the southwest) (Figure 9e).

4.3.2. Dushanzi Anticline

The Dushanzi anticline crops out on the surface at approximately 14 km north of the Tianshan mountain front (Figure 3a). Surface measurements (strike and dip) provide the opportunity to correlate field data with seismic subsurface data (Figure 10). On seismic profile Line 2, the anticline was largely asymmetric, with a gently dipping (21°–38°) southern backlimb and a much narrower and steeper (58°–67°) northern forelimb, even locally overturned (Figure 10a). Many researchers had investigated the Dushanzi structure (Burchfiel et al., 1999; Charreau et al., 2018; W. Chen et al., 2012; Molnar et al., 1994; Poisson & Avouac, 2004; Su et al., 2018). In particular, Li et al. (2020)

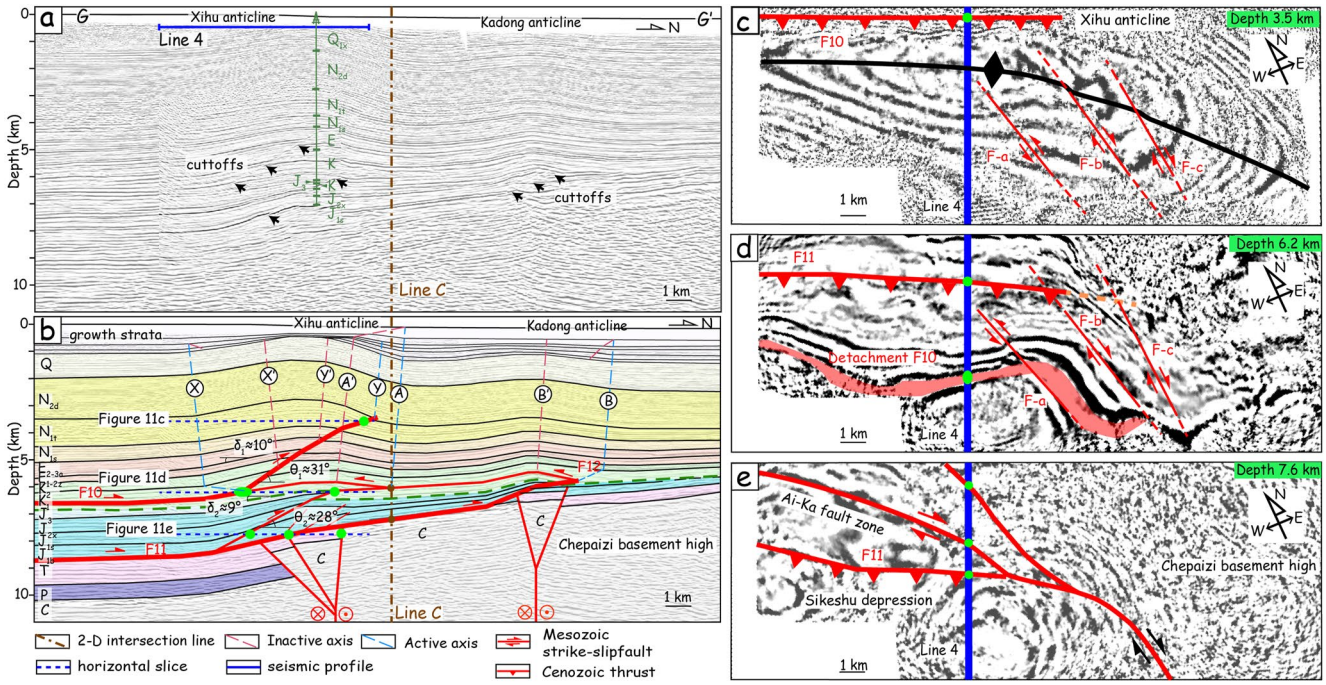

Figure 11. Structural analysis of the Xihu and Kadong anticlines. (a) Uninterpreted line across the Xihu and Kadong anticlines composed of 2-D regional line 4 and line G-G' (see Figure 1c for locations). (b) Interpreted seismic profile. Each fold overlies a triangle zones and two detachments: F11 at the base of the Jurassic, and F10 in the Cretaceous. Two sets of steeply dipping, strike-slip faults that form flower structures are interpreted below detachment F11. (c) Horizontal seismic slice at 3.5 km depth, illustrating the E-striking Thrust 10 and the curved, NW-trending fold trace of the Xihu anticline. (d) Horizontal seismic slice at 6.2 km depth, illustrating the E-striking Thrust 11 and detachment F10 whose east segment is bent. (e) Horizontal seismic slice at 7.6 km depth, showing Thrust 11 and the NW-striking Ai-Ka strike-slip fault which separates the Chepaizi basement high from the Sikeshu depression.

interpreted the Dushanzi anticline as a fault-propagation fold (FPF) related to thrust F8 that roots at depth onto a mudstone *décollement* layer from the Cretaceous Tugulu Group (K_{ltg}) (Figure 10b). We adopted this interpretation and further identified a secondary thrust F9 below F8. Both fault sole into the same Cretaceous *décollement*.

We then applied the forward trishear FPF modeling technique within Structure Solver© software to constrain our interpretation of the shallow fold (Erslev, 1991; Suppe & Medwedeff, 1990). In our model (Figure 10c), several tests converged to a setting characterized by a 40° southward dipping fault F8 (θ_1), a trishear angle of 76°, an inclined shear angle of 81°, and a propagation-to-slip ratio (P/S) of 0.52. The best fit was achieved when the horizontal shortening was approximately 5.8 ± 1.45 km. A movie of the structural modeling for the Dushanzi anticline was available in the supplementary material (Movie S1). The geometry of the growth strata predicted by the forward model was consistent with the growth strata mapped on the seismic profile (blue layers in Figure 10c). This indicated that the anticline nucleated during the deposition of the upper Miocene Dushanzi Formation and has been structurally growing since the deposition of the Pliocene to the Quaternary ($N_{2d} + Q$) strata.

In addition, we proposed that a positive flower structure affected the folding of the Mesozoic strata below and ahead of the upper FPF. To the south of the fault was the basin that deposited Permian, Triassic, and Jurassic strata, while to the north were the CBH Paleozoic basement and Jurassic lateral cover (Figure 10b). Note that, here, this flower structure folded the Cretaceous unconformity and the overlying Eocene series, which indicated that it was active in Neogene period.

According to the forward modeling of the shallow FPF and our interpretation of the deep positive flower structure, we proposed a new kinematic model for the Dushanzi structure (Figure 10d). First, during the Jurassic period, the Ai-Ka Fault cut through the Jurassic strata, and was covered by Cretaceous - Paleogene sediments. Until the middle Miocene, no tectonic deformation is documented since layer thicknesses are constant across the Dushanzi area. Finally, since the Middle-Upper Miocene, the Ai-Ka Fault reactivated and folded the Cretaceous - Paleogene strata. Simultaneously, thrust fault developed along the Cretaceous *décollement* layer, forming the thin-skinned Dushanzi anticline.

The 5 km-depth horizontal slice intersected with the shallow FPF and thrusts F8 and F9, and illustrated the near E-W strike of these structures (Figure 10e). Deeper, the 8 km-depth horizontal slice intersected with the flower structure and showed a set of three NW-SE fault traces (Figure 10f).

4.3.3. Xihu and Kadong Anticlines

4.3.3.1. Structure in 2D Cross-Section and Map-View

Located to the north of the Dushanzi anticline, the Xihu and Kadong anticlines are approximately 21.5 and 31 km away from the Northern Tianshan mountain front, respectively (Figure 3a). The Xihu anticline is exposed at the surface with a gentle relief, whereas the Kadong anticline is buried. We used a composite seismic profile G-G' and Line 4 (extracted from 3D seismic data) to investigate the subsurface geology of both anticlines (Figure 11a). They both developed above two triangular zones associated with a long and gently south-dipping basal detachment (F11) along the bottom of Jurassic units (Figure 11b).

In detail, the Xihu anticline was an asymmetric fold with a large, gently dipping southern backlimb and a narrow northern forelimb. It was a composite imbricate structure formed by the superimposition of two structures. Indeed, two rows of cutoffs indicated two south-dipping thrust ramps rooted in two distinct detachment levels (Figure 11a). The upper thrust ramp rooted onto detachment F10 within the lower Cretaceous (K_1), whereas the lower thrust ramp rooted onto detachment F11 within the Lower Jurassic Badaowan Formation (J_{1b}) (Figure 11b). Along the shallow detachment F10, the fault slip decreased to zero at the thrust tip, and the rest of the displacement was consumed by folding. We interpreted this shallow anticline as a shear FPF (Suppe & Medwedeff, 1990). Indeed, the backlimb dip ($\delta_1 = 10°$) was much lower than that of the thrust ramp ($\theta_1 = 31°$), and the Lower Cretaceous series (K_1) thickens above the detachment, suggesting simple shear along detachment F10. Along the basal detachment and ramp F11, a structural wedge deformed the shallow Xihu anticline and folded the upper thrust ramp, resulting in a kink band between axial surfaces A and A'. Below the basal detachment, a flower structure bounded by two sets of steeply dipping faults was interpreted to limit the southern Permian to Jurassic basin to the Northern CBH.

The Kadong anticline was a more symmetric fold with a structural wedge at its core. This structural wedge was controlled by a deep fault (F11) and a shallow fault (F12). The deep fault (F11) thrusted northward above the basement structure, connected with fault F12 at the tip of the structural wedge, and then thrusted southward along the detachment layer of the Lower Cretaceous (K_1). We interpreted the basement structural feature as a positive flower structure bounded by two steeply dipping faults that offset the Permian to Jurassic (Figure 11b).

Three horizontal slices extracted from the Xihu 3-D seismic data (Figures 11c, 11d, 11e) illustrated the vertical spatial evolution of the Xihu structure and the relationship between the shallow fold and the deep flower structures. The 3.5 km-deep horizontal slice (Figure 11c) intersected with the shallow Xihu anticline and the F10 shallow thrust ramp (Figure 11b). The anticline exhibited a curved fold axis that turns from W-E in the western part to WNW-ESE in the eastern part. The shallow thrust ramp (F10) strikes W-E. Three NW-striking tear faults (F-a, F-b, F-c) with apparent strike-slip motion were present at the eastern hinge of the Xihu fold. Fault F-a displayed a left lateral offset of markers, whereas F-b and F-c present a right-lateral offset. At 6.2 km depth (Figure 11d), the horizontal slice intersected with detachment F10 and the deep thrust ramp F11. The trace of detachment F10 was sinuous with a W-E bulk strike in the western part, whereas it turned to NW-SE in the eastern section. Deep thrust ramp F11 striked W-E in the western section of the fold, that was parallel to the F10 detachment. The three faults of the eastern Xihu hinge, F-a, F-b, and F-c, were still visible. These faults offset beddings at northwestern fault's tip, but they became parallel to beddings toward southeastern tip. At 7.6 km depth (Figure 11e), the horizontal slice intersected with the F11 thrust ramp and illuminated the steeply dipping faults of the basement flower structure (Figure 11b).

Thanks to the three horizontal slices (Figures 11c, 11d, and 11e), we established the 3D structure of the Xihu anticline and the link between the shallow and deep structures. Indeed, in the western part, the shallow, E-W Xihu fold was parallel to thrust ramps F10 and F11. In the eastern part, the trace of detachment F10 turned and becomes parallel to the NW-SE Ai-Ka fault trace. This suggested that the deep basement structure may have governed the orientation of the eastern Xihu fold by controlling the strike of detachment F10. NNW-SSE tear faults (F-a, F-b, F-c) would be linked to the lateral ramp in the F10 detachment level and the accommodation of the bending of the fold axis in the transition zone between the western and eastern segments.

10.1029/2023TC007986

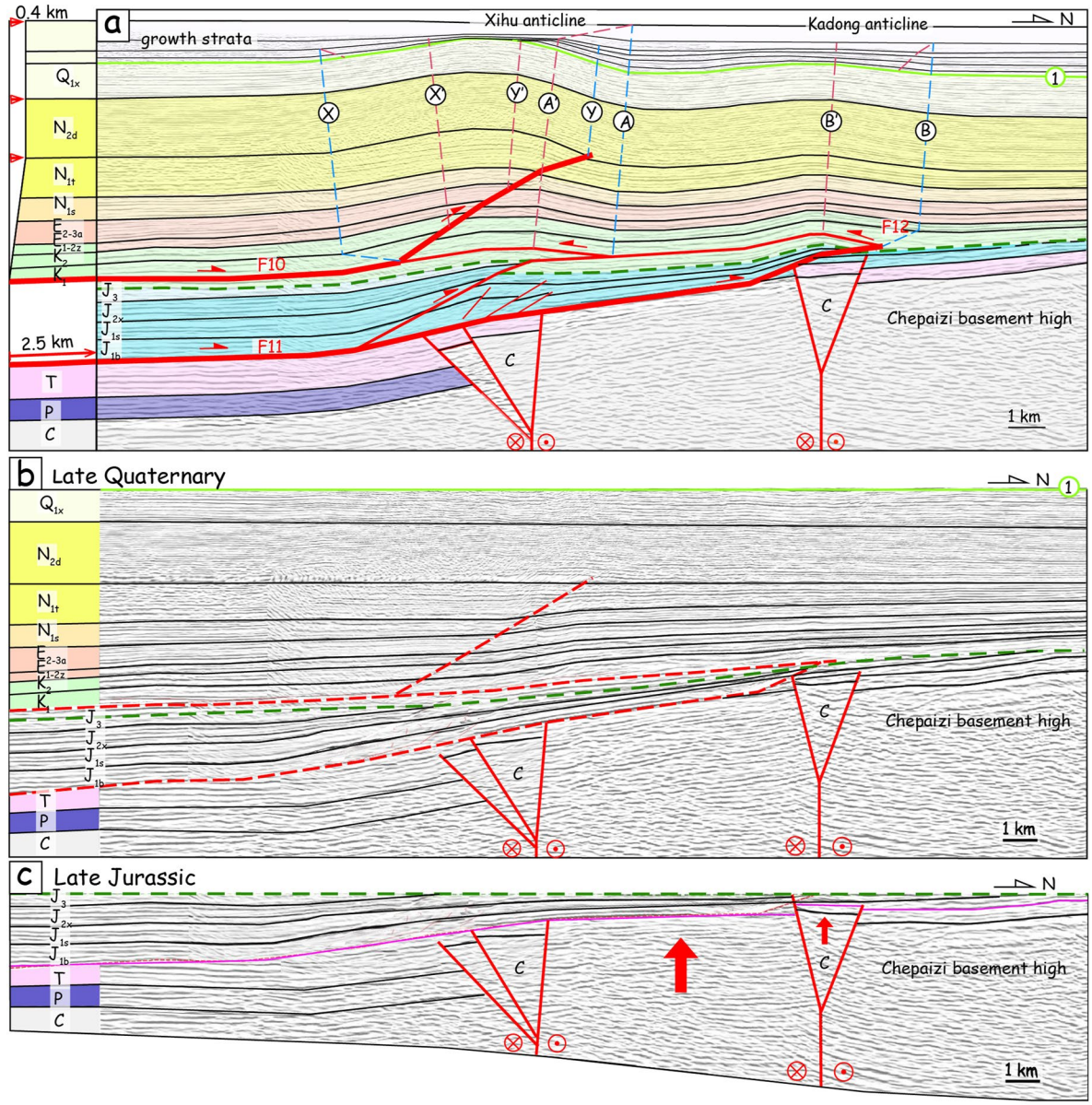

Figure 12. Balanced sequential restoration of the Xihu and Kadong anticlines. (a) Structural interpretation of the Xihu and Kadong anticlines at present. Red solid lines indicate active faults. Red dashed lines show the fault trajectory prior to displacement. (b) Restored seismic profile by flattening layer 1 (in green). Note that 0.4 km of displacement on detachment F10 has been restored and was consumed in the shallow Xihu anticline. A total shortening of 2.5 km displacement is restored along detachment F11. The thicknesses of the Xiyu Formation (Q_{1x}) and Dushanzi Formation (N_{2d}) are constant from south to north. Instead, the Cretaceous (K) to Taxihe Formations (N_{1t}) becomes thinner toward the north. (c) Restored seismic profile in the Late Jurassic. The basement rock and the flower structure at Kadong were uplifted.

4.3.3.2. Restoration

The kinematics of the Xihu and Kadong anticlines can be inferred from the growth strata above Quaternary layer 1 (bright green—Figure 12a). Both structures displayed two growth triangles on their northern limb, bounded by axial surfaces A and A' and B and B', respectively (Figure 12a). We restored the Xihu and Kadong seismic profile G-G' by flattening the growth strata layer. We presented three stages, from the present to the Late Jurassic (Figure 12).

First, after being flattened to the bright green Quaternary marker, both the Xihu and the Kadong anticlines were fully unfolded, indicating the simultaneous formation of these two anticlines (Figures 12a and 12b). Approximately 2.5 ± 0.6 km of shortening had been consumed by both anticlines along the F11 detachment. Additionally,

0.4 ± 0.1 km of shortening had also been consumed in the shallow Xihu anticline by detaching on the shallow F10 detachment. The constant thickness of the Xiyu (Q_{1x}) and Dushanzi (N_{2d}) Formations indicated no structural movement during the Late Miocene to Early Quaternary. However, the Cretaceous to Taxihe Formations (N_{1t}) thins northward, which indicates that the CBH slightly uplifted (or the Sikeshu depression subsided) from Late Cretaceous to Late Miocene.

Then, we removed the Cretaceous to Quaternary beddings and flattened the Cretaceous unconformity to obtain the structures in the Late Jurassic period (Figure 12c). Important uplift of the CBH during the Jurassic was illustrated by (a) the south-dipping Triassic-Jurassic bedding in the Xihu area, (b) the positive flower structure in the Kadong area that cut off the Triassic and Lower Jurassic horizons, and (c) truncation of Jurassic layers above the CBH.

To summarize, deformation along this geological section started first with the deep positive flower structures that bent the Triassic-Jurassic beddings in the Xihu area and faulted the Lower Jurassic *décollement* level in the Kadong area. Then, during the late Quaternary, the bend point in Xihu and the *décollement* cut-off in the Kadong behaved as a mechanically weak zone that favored a thrust ramp under contractional conditions, nucleating a long structural wedge that activated the deep F11 Jurassic and shallow F10 Cretaceous *décollements* (Figures 12a and 12b). Simultaneously, there was no tectonic reactivation of the basement flower structures since the geometry of these flower structures barely changed before and during the activity of the Xihu and Kadong anticlines. Only 3° of southward tectonic tilting occurred from the Cretaceous to early Miocene times, as recorded by the slope of the Cretaceous unconformity (Figure 12b).

4.3.4. Kayindike Anticline

The Kayindike anticline is a buried anticline located 40 km away from the northern Tianshan front and at the northwestern end of the Ai-Ka structure system (Figure 3a). Our interpretation of seismic profile Line 5 extracted from the 3D seismic data (Figure 13a and Figure 5) showed that the Kayindike anticline was a simple fault-bend fold (Figure 13b). The major thrust (F4) ramped over a positive basement relief and exhibited a flat-ramp-flat geometry, which propagated upward from the basal detachment (F4) in the Lower Jurassic Badaowan Formation (J_{1b}) to the Cretaceous unconformity (Figure 13b). Consistent with the fault-bend fold model (Suppe, 1983), the width of the X-X' kink band equaled the displacement along the basal flat. Therefore, approximately 1.9 ± 0.47 km of displacement had been input into this structure along the thrust fault. The rest of the displacement continued to transfer toward the CBH along the upper *décollement*, since outside the range of Line 5, tiny folds still occurred further north, which was likely to consume the rest of the displacement.

Based on the above geometry and kinematic analysis of the Kayindike anticline (Figure 5), we proposed 2-D balanced forward modeling (Figure 13c) that sketched the evolution of the Kayindike deformation from the Late Jurassic to the present. First, during the Jurassic (Figure 13c-1), the northern side of the flower structure (i.e., CBH) was active and uplifted. A Jurassic basin developed to the south in the Sikeshu depression with a presumably northward decrease in layer thickness above the CBH. At the Late Jurassic, regional erosion flattened the topographic surface and truncated the Jurassic beddings, leading to an unconformity. From the Cretaceous to Early Pliocene (Figure 13c-2), Paleogene to Neogene layers covered unconformably the pre-Cretaceous basin and the CBH. Finally, from the Late Quaternary until the present (Figure 13c-3), a thrust fault propagated northward along the basal detachment in the Lower Jurassic (J_{1b}), and the deformation reached the frontal erosional tip (pinch-out) of the *décollement* level that moved upward along the Cretaceous unconformity surface. The pinch-out of *décollement* surface triggered the causative thrust ramp of the Kayindike anticline.

In the Kayindike 3-D seismic data, a horizontal slice at approximately 4-km depth (Figure 13d) intersected with a shallow anticline (see the slice level in Figure 13b). It illuminated a NW-SE anticline with a sharp overlap/relay zone in the middle of the structure. The deeper 6-km depth horizontal slice (Figure 13e) intersected with the basal detachment F4 and the basement flower structure (compare this slice level with the section in Figure 13b). The traces of detachment F4 and the Ai-Ka basement fault were parallel and strike NW-SE. The basement fault separated the CBH to the northeast from the Sikeshu depression to the southwest.

In brief, the shallow and deep observations observed at the Kayindike structure suggested that the deep flower structure in the basement controlled the development of the shallow folded structure. The main Jurassic *décollement* (F4) involved in the growth of the shallow fold was folded during the Late Jurassic deformation prior to its activation during the Quaternary compression. Therefore, the localization of the Quaternary deformation and the strike of the shallow, young thrusts and related folds were directly inherited from the Mesozoic deformation that folded the *décollement* level.

10.1029/2023TC007986

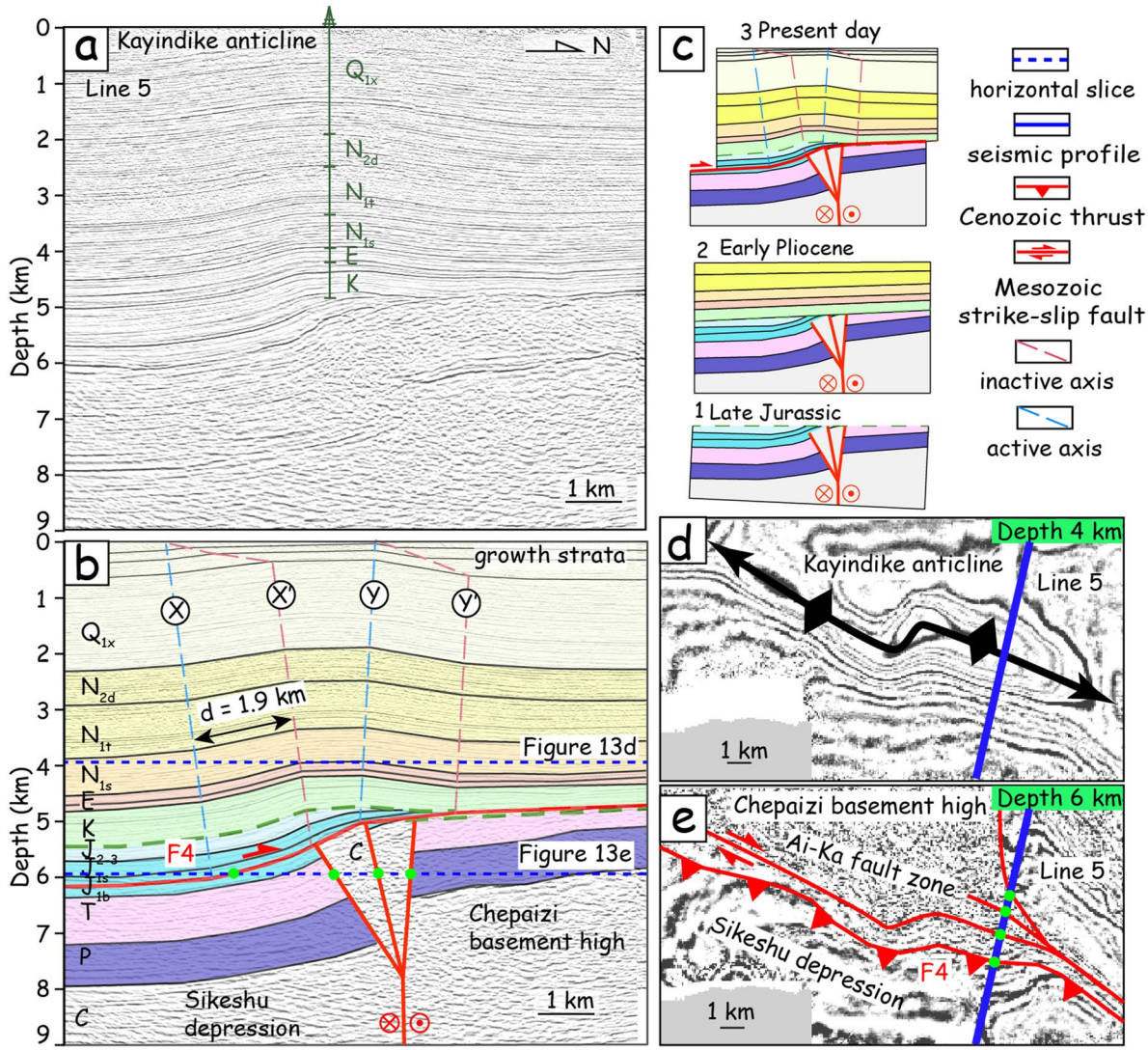

Figure 13. Structural analysis of the Kayindike anticline. (a) Uninterpreted line 5 across the Kayindike anticline (refer to Figure 1c for location). (b) Interpreted seismic profile of the Kayindike anticline, with the interpretation of a fault-bend fold characterized by a north-verging flat-ramp-flat thrust fault stepping up from the Lower Jurassic Badaowan Formation (J_{1b}) to the Cretaceous basal unconformity. The kink band width XX' suggests that thrust F4 accommodates 1.9 km of fault slip. Beneath the anticline, a steeply dipping fault cuts off the Paleozoic, Triassic, and Jurassic strata and forms a positive flower structure. (c) Evolution sketch of the Kayindike anticline with three stages: Late Jurassic, Early Pliocene, and present. (d) Horizontal seismic slice at 4-km depth, illustrating the fold trace of the NW-trending Kayindike anticline. (e) Horizontal seismic slice at 6-km depth, highlighting Thrust 4 that is parallel with the NW-striking Ai-Ka fault zone, which separates the Chepaizi basement high from the Sikeshu depression.

4.4. The Sikeshu Depression Between the Gaoquan and Ai-Ka Structural Belts

The Sikeshu depression is a ~9 km-deep depocenter between the Gaoquan structure to the west and the Ai-Ka structure belt to the east (Figures 3b and 3c). In map view, seismic depth slices showed at least two syncline branches: An E-W to SW-NE curved axis to the west and a NW-SE straight axis to the east (Figure 3b). These axes can be traced from the shallow level (Figures 3b, 9d, and 10e) to the deeper depth (Figures 3c, 9e, and 10f), indicating that the Sikeshu depression was a first-order feature within the Northern Tianshan foreland basin.

We analyzed a SW-NE-oriented seismic line (Line 3) across the Sikeshu depression to study its structure at depth (Figure 14). The Sikeshu depression appeared as a structurally transported basin (piggy-back basin) bounded by the Tianshan range front to the southwest and the Dushanzi anticline to the northeast. It displayed a clear concave-upward shape of thick Neogene to Quaternary layers in the center, and it was transported over two thrusts: a shallow thrust (F8) associated with the Dushanzi anticline, and a deeper thrust (F14) that offset the

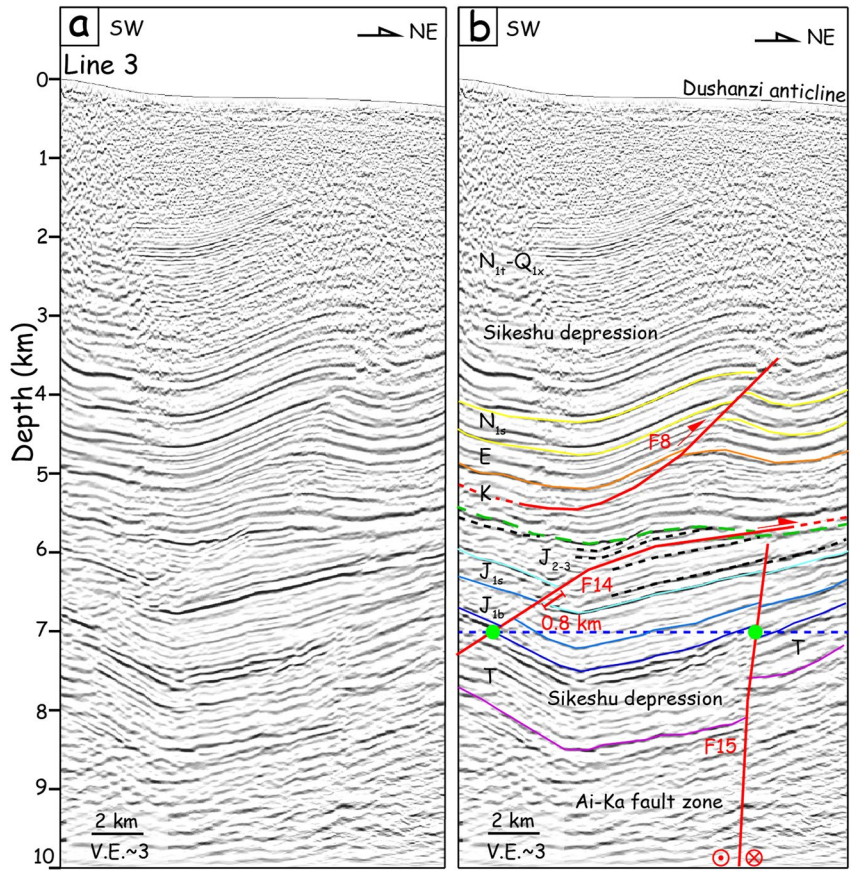

Figure 14. Geometry of the Sikeshu depression. (a) Uninterpreted seismic profile Line 3. (b) Interpreted seismic profile Line 3 (see Figure 1c for location). The Dushanzi anticline has been deformed by thrust F8, while the footwall of fault F8 has been folded by a ramp-flat thrust F14. The steeply dipping fault trace (F15) offset the Triassic-Jurassic beddings. Green dots annotate the intersection points between the horizontal seismic slices (blue dashed line) and the Cenozoic thrust (F14) and Ai-Ka fault zone (F15), which can also be seen in Figure 10f at 8-km depth.

Jurassic beddings by 0.8 ± 0.2 km on fault. In the footwall of the deep F14 ramp-flat thrust, a steeply dipping fault (F15) belonging to the Ai-Ka strike-slip fault zone offset the Triassic to Jurassic beddings and was sealed by the Cretaceous unconformity. These observations suggested that fault F15 was active in the middle to late Jurassic and had ceased since the Cretaceous. Based on this information, we suggested that the pre-Cretaceous depocenter of the Sikeshu depression was controlled by the Ai-Ka fault zone.

5. Discussion

5.1. Geometry and Kinematics of the Mesozoic Strike-Slip Structures

The Mesozoic structures along the Tianshan range had undergone extensive investigations (e.g., Allen & Vincent, 1997; Choulet et al., 2011; Laurent-Charvet et al., 2002; Shu et al., 1999). Low-temperature thermochronological data obtained within the Tianshan and adjacent areas, coupled with thermal history modeling, revealed multiple cooling events during the Mesozoic period. These events were interpreted as denudational responses to tectonic uplift (Bullen et al., 2001, 2003; De Grave & Van den haute, 2002; De Grave et al., 2014; Dumitru et al., 2001; Jolivet et al., 2001). These events had supplied detrital sediments for several Mesozoic intermountain basins, sealed by a widespread angular unconformity at the Early Cretaceous (De Grave et al., 2007; Hendrix, 2000; Hendrix et al., 1992). However, the structural characteristics of the Mesozoic tectonics, encompassing geometry, kinematics, and timing, remain inadequately documented.

Building upon seismic interpretation and balanced restoration results, we demonstrate the dominance of wrench tectonics in the western region of the Northern Tianshan foreland basin during the Triassic and Jurassic periods.

We identified two sets of strike-slip fault zones in the Ai-Ka and Gaoquan areas characterized by either positive or negative flower structures on cross-sections (see Figures 4–7, 10, 11, 13).

The subsequent discussion focused on the kinematics of these two strike-slip fault zones. The determination of the sense of strike-slip motion in a wrench fault system was classically based on observing structural geometry in relay zones. For instance, the presence of negative flower structures in releasing bends in a right-step pattern indicates dextral faulting, while positive flower structures in restraining bends signify sinistral faulting (Aydin & Nur, 1982; Mann et al., 1984; K. McClay & Bonora, 2001; Segall & Pollard, 1980; Sylvester, 1988); the opposite holds for the left-step pattern. This has been documented along various wrench systems, such as the San Andreas Fault (Bergh, et al., 2019; Dair & Cooke, 2009; Schwartz et al., 1990), the North Anatolian Fault (Armijo et al., 1999; Aydin & Nur, 1982; Barka & Kadinsky-Cade, 1988), the Levant Fault (Ghalayini et al., 2014; Gomez et al., 2007; Le Pichon & Gaulier, 1988), and the Altyn-Tagh Fault (Elliott et al., 2018; Xiao et al., 2017). Numerous analog and numerical models have also validated such geometric-kinematic relationships (Boussarsar et al., 2022; T. Dooley & McClay, 1997; T. P. Dooley and Schreurs et al., 2012; Emmons, 1969; K. McClay & Bonora, 2001; K. McClay & Dooley, 1995; Richard et al., 1995; Wu et al., 2009).

In the Ai-Ka fault zone, major basement fault segments were arranged in right steps on the map, with negative flower structures observed at the relay zone between the major fault segments (e.g., Lines A and C—Figures 3c and 4). These observations indicated that the Ai-Ka fault zone was a right-lateral strike-slip system. The sedimentation architecture observed in Figure 4a supported that Ai-Ka fault zone was active during the pre-Cretaceous period. The Triassic to Jurassic beddings filled the negative flower structure and thicken toward the high-angle fault trace, suggesting that the Ai-Ka fault zone controlled the geometry of the syntectonic deposition during this time.

In the Gaoquan fault zone, two major faults (f1 and f2) exhibited a right-step pattern on the map (Figure 3c), and seismic profile (Line 6) displayed a positive flower structure in the relay zone between f1 and f2 (Figure 6b). These features aligned with a restraining bend in a left-lateral strike-slip fault zone (K. McClay & Bonora, 2001). Restoration of the Gaoquan structure suggested that this strike-slip fault zone was active during Jurassic, concurrent with the Ai-Ka fault zone (Figure 7e). The thinning of Lower Jurassic strata onto the top of the pop-up structure further supported this observation.

Between the Ai-Ka and Gaoquan strike-slip fault zones, the cross-sectional geometry of the Sikeshu depression was controlled by the steeply dipping fault (F15) within the Ai-Ka strike-slip fault zone (Figures 10f and 14b). Mesozoic strike-slip faulting was also evidenced along the Dunan structure during the Jurassic (Figure 9c). This suggested that during the Pre-Cretaceous periods, the western Northern Tianshan foreland was dominated by right-lateral strike-slip faulting: the NTF in the south range front and the Ai-Ka fault zone in the north, resulting in the formation of the Sikeshu depression. Along these strike-slip structures, several pop-up/positive flower structures, such as Gaoquan, developed as restraining bends. Therefore, the Sikeshu depression subsided, whereas structures such as Gaoquan or those along the Ai-Ka fault zone were uplifted simultaneously. Meanwhile, the CBH, located northeast of the Ai-Ka fault zone, was uplifted relative to the Sikeshu depression (Figure 15a). Low-temperature thermochronology data also documented limited cooling events and the deposition of coal strata coexisting in the southern Junggar basin during the Jurassic (Dumitru et al., 2001; Jolivet et al., 2010; W. Yang et al., 2013). This feature was consistent with the strike-slip tectonics scenario identified in the western region of southern Junggar basin.

To explain the opposite sense of movement and the 60° angle between the right-lateral Ai-Ka and the left-lateral Gaoquan strike-slip structures during the Pre-Cretaceous, we used the classic Riedel shear model (Cloos, 1928; Riedel, 1929; Tchalenko, 1970). In the Riedel right shear model, when conjugate faults develop in an overall right-lateral shear setting, R-shear displays right-lateral motion, whereas R'-shears display left-lateral motion, and the internal angle in-between is approximately 60° (G. H. Davis, et al., 2000; Sylvester, 1988). Thus, we suggested that during the Pre-Cretaceous, the western region of the Northern Tianshan foreland basin was dominated by a large-scale right-lateral shear zone. This regime formed the Ai-Ka right-lateral strike-slip fault zone that contributed, along with the right-lateral NTF, to the development of the Sikeshu depression as a large complex pull-apart basin. This shear zone regime also caused the Gaoquan left-lateral strike-slip fault zone as the conjugate R'-type shear to the major R-type Ai-Ka shear (Figure 15a).

5.2. Effects of Structural Inheritance on Cenozoic Shortening

Our seismic interpretations showed two types of structural interactions between the deep Mesozoic tectonics and the shallow Cenozoic-Quaternary tectonics.

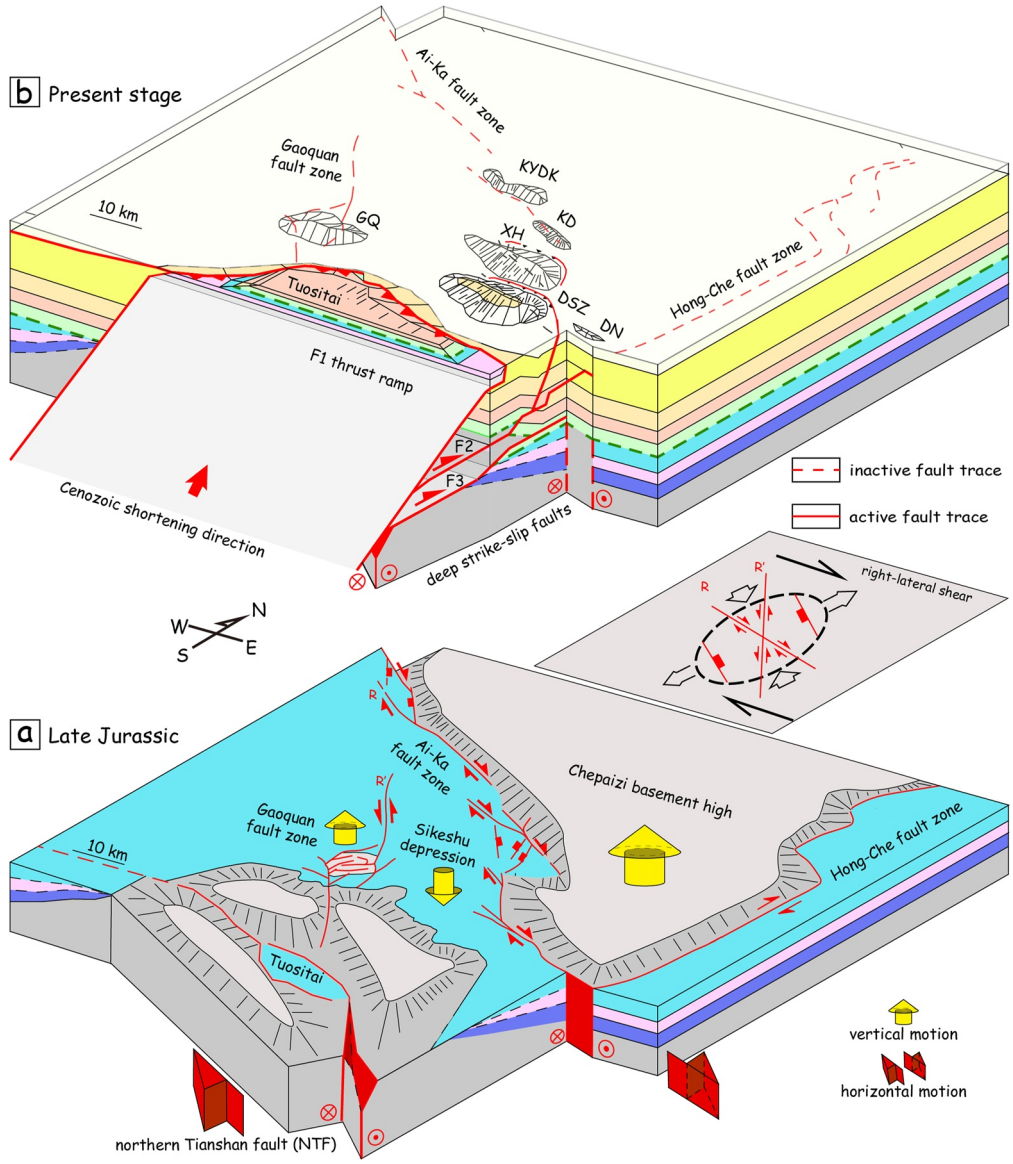

Figure 15. Three-dimensional sketch of the tectonic evolution in the Late Jurassic and present stage. (a) 3-D sketch of the Ai-Ka, Hong-Che, and Gaoquan strike-slip faults. The NW-striking Northern Tianshan fault (NTF) and Ai-Ka fault zone compose a right lateral shear zone, in which the Gaoquan left-lateral restraining bend was developing. To the north, the Chepaizi basement high was bounded by active strike-slip faults and underwent relative uplifting. For comparison, the insert chart shows a theoretical Riedel shear model, in which the NTF and Ai-Ka fault zones represent *R*-shear and the Gaoquan fault zone represents *R'*-shear in the right-lateral shear zone. (b) 3D sketch of the Cenozoic thrust-related folds. The Tuositai structure belt comprises a thrust nappe, which is offset by a south-dipping thrust (F1) and uplifted to the surface. The Gaoquan (GQ) anticline is parallel to the thrust nappe. The NW-striking Ai-Ka structure belt is composed of the Dunan (DN), Dushanzi (DSZ), Xihu (XH), Kadong (KD), and Kayindike (KYDK) anticlines, which are arranged in an "*en échelon*" map-view pattern.

In the first type, some Cenozoic thrust ramps localized above the basement Mesozoic structural relief due to an interruption in the *décollement*. This interruption, a pinch-out in the *décollement* continuity (Costa & Vendeville, 2002), can have either a structural origin, as observed in Dunan and Kadong anticlines (Figures 9c and 11b), or an erosional origin, as seen in Kayindike anticline (Figures 13b and 13c). In both cases, the pinch-out in the *décollement* level resulted from a flower structure or erosion, respectively, interrupting the detachment level's continuity. Despite the differing origins, the geomechanical effect was similar, as the interruption blocked the transmission of compressional stress within the detachment level, forcing the thrust to ramp upward and

Table 1
Quantitative Analysis of Nucleation Timing, Shortening Rate, and the Distance to the Tianshan Range Front for Each Anticline

	Distance to Tianshan range front (km)	Reactivation of basement structure	Thickness of quaternary sediments at the syncline	Average sedimentation rate of quaternary sediments	Thickness of growth strata	Shortening consumed in shallow structure		
						Period (my)	Magnitude (km)	Rate (mm/year)
Dunan	~7	No			~2.1	4.8–7.5	1.8	0.24–0.37
Gaoquan	~12.5	Yes			~1.5	4.8–7.5	1	0.13–0.20
Dushanzi	~14	Yes			~3.8	16	5.8	0.36
Xihu	~21.5	No	~2.0	0.26–0.41	~1.2	2.9–4.6	2.9	0.63–1.00
Kadong	~31	No	~2.1	0.29–0.45	~1.2	2.6–4.1		0.70–1.11
Kayindike	~40	No	~2.25	0.30–0.47	~0.72	1.5–2.4	1.9	0.80–1.26

Note. The lithostratigraphic age to calculate the shortening rate is based on the data from Charreau et al. (2005), Charreau, Gumiaux, et al. (2009), Charreau, Chen, et al. (2009), which is illustrated in Figure 2.

consume shortening into a fault-related fold. For example, beneath the Dunan anticline, a preexisting strike-slip fault forced thrust F6 to ramp upward (Figures 9b and 9c).

The second type of structural interactions involved the initiation and reactivation of Mesozoic positive flower structures during the early Cenozoic, influencing the folding of the main *décollement* level (Anjihaihe Formation level). This process, observed in the Gaoquan, Dushanzi, and the core of the Xihu anticline (Figures 7, 8, 10b, 10d, and 12), is a common phenomenon documented worldwide (e.g., Butler, 1989; Schedl & Wiltschko, 1987; Williams et al., 1989) in FTBs, such as the Jura Mountains (e.g., Homberg et al., 2002; Malz et al., 2020), the Alps and Alpine forelands (e.g., Bellahsen et al., 2014; Ziegler, 1989), the Apennines (e.g., Di Domenica et al., 2014; Scisciani, 2009), and the fossil Variscan belt (Laurent et al., 2021). Subsequently, along the strike of preexisting structures, these two types of structural inheritance expanded into three dimensions, influencing the strike of the younger thrust ramp and the spatial arrangement of thrust-related folding.

Based on our seismic interpretation, we constructed a 3-D structural model to showcase the spatial control of the deeper pre-Cretaceous strike-slip fault zones on shallower Neogene-Quaternary thrust-related anticlines (Figure 15). The orientation of shallow *en échelon* anticlines in the Ai-Ka structural system was consistent with the right-step *en échelon* strike-slip segments at depth. In the Gaoquan structural system, the location of the shallow anticline formed above a rounded basement high associated with a restraining bend (Figures 15a and 15b).

5.3. Displacement Consumption Along Shallow and Deep Structures

In this discussion, we systematically analyzed each shallow structure, including Gaoquan, Dunan, Dushanzi, Xihu, Kadong, and Kayindike anticlines in the western region of Northern Tianshan foreland basin, by documenting nucleation timing, calculating shortening amounts and rates (refer to Table 1), and summarizing their distances to the Tianshan range front, along with indications of basement structure reactivation. The primary objective was to assess how shortening has partitioned between shallow structures, considering the preexisting basement structures in the foreland basin.

Structures such as Gaoquan and Dushanzi, located within 15 km from the mountain front, showed potential for reactivation, as depicted in Figures 7 and 10. In contrast, structures farther north, like Xihu, Kadong, and Kayindike anticlines, did not exhibit evidence of reactivation of the deep basement flower structures (Figures 12 and 13b). This indicated that thick-skinned tectonics predominantly affect structures in close proximity to the main mountain front.

Examining the nucleation timing for each anticline revealed a progressive northward migration of thin-skinned tectonic deformation into the foreland. The S-N regional seismic profile restoration implied that the Neogene deformation of the Tuositai thrust nappe initiated in the Middle Miocene (Figure 5b). Meanwhile, the Dushanzi anticline deformed after the middle Miocene (16 Ma according to the magnetostratigraphic study from Charreau, Gumiaux, et al. (2009)). Subsequent deformation in Gaoquan and Dunan anticlines occurred during the Late Miocene-Pliocene (4.8–7.5 Ma). Further north, in the Quaternary, deformations extended to form the Xihu,

Kadong, and Kayindike anticline. This foreland propagation mode was consistent with findings from previous studies in the middle and eastern regions of the Northern Tianshan foreland basin (Burchfiel et al., 1999; Charreau et al., 2008; Daëron et al., 2007; H. Lu et al., 2009).

To quantitatively evaluate the impact of basement structures on subsequent contractional deformation, specifically in terms of shortening rate partitioning on the thin-skinned structures in the western Northern Tianshan foreland basin, we compared the amount of total shortening rate along three S-N structural profiles: The Gaoquan-Kayindike line, the Dushanzi-Xihu line, and the Dunan line. All the thin-skinned anticlines in these three structural lines initiated in the Late Pliocene-Quaternary, except the Dushanzi anticline (~16 Ma). Therefore, to compare the displacement rate among these lines, we assumed that the deformation rate of the Dushanzi anticline was stable. Based on this assumption, the total shortening rate was as follows: (a) 0.90–1.46 mm/yr along the Gaoquan-Kayindike structural line; (b) 0.96–1.36 mm/yr along the Dushanzi-Xihu structural line; and (c) 0.24–0.37 mm/yr along the Dunan line (Table 1).

The results indicated that the shortening rate was stable at the first two lines in the west and middle area of Sikeshu depression. However, a significant decrease of the shortening rate occurred at third line in the far eastern side. We attributed this to the narrow S-N width of the Sikeshu depression at the far eastern side, influenced by the deep NW-striking Ai-Ka strike-slip fault along the CBH margin.

This narrowing effect contrasted with the middle region of the Northern Tianshan foreland basin, where the wider S-N basin width facilitated higher Quaternary average shortening rate along the southern Junggar thrust for about 3.6 mm/yr (Qiu et al., 2019) and no basement structures hindering the propagation of thin-skinned deformation.

6. Conclusions

Based on the interpretation of 2-D and 3-D seismic data and balanced restoration profiles, we have characterized the evolution of the geometry and kinematics of shallow and deep structures in the western region of the Northern Tianshan foreland basin, northwestern China. The results showed the following:

1. Together with the Northern Tianshan strike-slip fault, the NW-trending Ai-Ka strike-slip fault controlled a right-lateral shear zone in the study area during the Jurassic. This shear zone initiated the Gaoquan left-lateral restraining bend and promoted the development of Sikeshu depression as a pull-apart basin.
2. The spatial arrangement of Cenozoic thrust-related folds along the Ai-Ka and Gaoquan structural belts was inherited from the Mesozoic strike-slip fault zones. The preexisting basement strike-slip fault zones localized the contractional stress and strain and forced the formation of the thrust ramp. This occurred (a) where the *décollement* was interrupted by a fault (structural pinch-out), erosion (erosional pinch-out), or (b) where the *décollement* was folded by activation of preexisting flower structures.
3. During the northward progressive migration of the thin-skinned tectonics in the Sikeshu depression, western region of the southern Junggar Basin, the total thin-skinned shortening rate decreased eastward from 0.96 to 1.36 mm/yr to 0.24–0.37 mm/yr. This was because, the preexisting NW-trending Ai-Ka strike-slip fault zone that characterized the margin of CBH, narrowed the S-N width of Sikeshu depression eastward, resulting in limiting the range of propagation of thin-skinned deformation.

Data Availability Statement

The digital topography data and surface geology data used for creating Figure 1 are presented as supplementary figures, which can be downloaded from the following link (https://doi.org/10.6084/m9.figshare.19160966.v4).

Details about structural modeling, structural restoration, and area-depth-strain analysis techniques are available from StructureSolver User Workshop 4.1 from the following link (https://doi.org/10.6084/m9.figshare.20444976.v1).

Acknowledgments
Many thanks to Dr. Julien Charreau for the insightful discussion and Dr. Liu Yiduo for reading our manuscript for language. We are grateful to the editor Dr. Marc Jolivet and two anonymous reviewers for their constructive suggestions. We highly appreciate the Xinjiang Oilfield Company, PetroChina, for providing the seismic database and well-log data. This work was supported by the National Natural Science Foundation of China (No. 41472183), the National Science and Technology Major Project of China (No. 2016ZX05047-001), and the Major Project of PetroChina (No. 2017E0403). Finally, we pay our highest respects to Pr. Bruno C. Vendeville, the fourth author, passed away during the manuscript revision. Bruno made significant contributions to this research in terms of the 3-D seismic interpretation. His avid guidance provided invaluable support to the first author, playing an indispensable role in refining this work.

References

Allen, M. B., Natal'in, B., & Natal'in, B. A. (1995). Junggar, Turfan and Alakol basins as late Permian to? Early Triassic extensional structures in a sinistral shear zone in the Altaid orogenic collage, central Asia. *Journal of the Geological Society*, *152*(2), 327–338. https://doi.org/10.1144/gsjgs.152.2.0327

Allen, M. B., & Vincent, S. J. (1997). Fault reactivation in the Junggar region, northwest China: The role of basement structures during Mesozoic-Cenozoic compression. *Journal of the Geological Society*, *154*(1), 151–155. https://doi.org/10.1144/gsjgs.154.1.0151

Allen, M. B., Windley, B. F., & Chi, Z. (1991). Active alluvial systems in the Korla basin, Tien Shan, northwest China: Sedimentation in a complex foreland basin. *Geological Magazine*, *128*(6), 661–666. https://doi.org/10.1017/S0016756800019750

Armijo, R., Meyer, B., Hubert, A. l., & Barka, A. (1999). Westward propagation of the North Anatolian Fault into the northern Aegean: Timing and kinematics. *Geology*, *27*(3), 267–270. https://doi.org/10.1130/0091-7613(1999)027<0267:wpotna>2.3.co;2

Avouac, J.-P. (1993). Analysis of scarp profiles: Evaluation of errors in morphologic dating. *Journal of Geophysical Research*, *98*(B4), 6745–6754. https://doi.org/10.1029/92jb01962

Avouac, J.-P., Tapponnier, P., Bai, M., You, H., & Wang, G. (1993). Active thrusting and folding along the northern Tien Shan and Late Cenozoic rotation of the Tarim relative to Dzungaria and Kazakhstan. *Journal of Geophysical Research*, *98*(B4), 6755–6804. https://doi.org/10.1029/92jb01963

Aydin, A., & Nur, A. (1982). Evolution of pull-apart basins and their scale independence. *Tectonics*, *1*(1), 91–105. https://doi.org/10.1029/TC001i001p00091

Barka, A. A., & Kadinsky-Cade, K. (1988). Strike-slip fault geometry in Turkey and its influence on earthquake activity. *Tectonics*, *7*(3), 663–684. https://doi.org/10.1029/TC007i003p00663

Bazhenov, M. L., Burtman, V. S., & Dvorova, A. V. (1999). Permian paleomagnetism of the Tien Shan fold belt, Central Asia: Postcollisional rotations and deformation. *Tectonophysics*, *312*(2), 303–329. https://doi.org/10.1016/S0040-1951(99)00181-X

Bellahsen, N., Mouthereau, F., Boutoux, A., Bellanger, M., Lacombe, O., Jolivet, L., & Rolland, Y. (2014). Collision kinematics in the western external Alps. *Tectonics*, *33*(6), 1055–1088. https://doi.org/10.1002/2013TC003453

Bergh, S. G., Sylvester, A. G., Damte, A., & Indrevær, K. (2019). Polyphase kinematic history of transpression along the Mecca Hills segment of the San Andreas fault, southern California. *Geosphere*, *15*(3), 901–934. https://doi.org/10.1130/ges02027.1

Bonini, L., Basili, R., Toscani, G., Burrato, P., Seno, S., & Valensise, G. (2015). The role of preexisting discontinuities in the development of extensional faults: An analog modeling perspective. *Journal of Structural Geology*, *74*, 145–158. https://doi.org/10.1016/j.jsg.2015.03.004

Boussarsar, M., Vendeville, B. C., Abbes, C., Hassine, M., & Ferrer, O. (2022). Analog modeling of the role of salt in the structuration of thin-skinned pull-apart basins: The case study of El Hamma basin, Central Tunisia. *Journal of Structural Geology*, *161*, 104634. https://doi.org/10.1016/j.jsg.2022.104634

Bullen, M. E., Burbank, D. W., & Garver, J. I. (2003). Building the northern Tien Shan: Integrated thermal, structural, and topographic constraints. *The Journal of Geology*, *111*(2), 149–165. https://doi.org/10.1086/345840

Bullen, M. E., Burbank, D. W., Garver, J. I., & Abdrakhmatov, K. Y. (2001). Late Cenozoic tectonic evolution of the northwestern Tien Shan: New age estimates for the initiation of mountain building. *GSA Bulletin*, *113*(12), 1544–1559. https://doi.org/10.1130/0016-7606(2001)113<1544:lcteot>2.0.co;2

Burchfiel, B. C., Brown, E. T., Qidong, D., Xianyue, F., Jun, L., Molnar, P., et al. (1999). Crustal shortening on the margins of the Tien Shan, Xinjiang, China. *International Geology Review*, *41*(8), 665–700. https://doi.org/10.1080/00206819909465164

Buslov, M. M., Watanabe, T., Fujiwara, Y., Iwata, K., Smirnova, L. V., Safonova, I. Y., et al. (2004). Late Paleozoic faults of the Altai region, central Asia: Tectonic pattern and model of formation. *Journal of Asian Earth Sciences*, *23*(5), 655–671. https://doi.org/10.1016/S1367-9120(03)00131-7

Butler, R. W. H. (1989). The influence of preexisting basin structure on thrust system evolution in the Western Alps. *Geological Society, London, Special Publications*, *44*(1), 105–122. https://doi.org/10.1144/GSL.SP.1989.044.01.07

Butler, R. W. H. (2017). Basement-cover tectonics, structural inheritance, and deformation migration in the outer parts of orogenic belts: A view from the western Alps. In *Linkages and Feedbacks in orogenic systems*.

Butler, R. W. H., & Paton, D. A. (2010). Evaluating lateral compaction in deepwater fold and thrust belts: How much are we missing from "nature's sandbox". *Geological Society of America Today*, *20*, 4–10. https://doi.org/10.1130/gsatg77a.1

Butler, R. W. H., Tavarnelli, E., & Grasso, M. (2006). Structural inheritance in mountain belts: An Alpine–Apennine perspective. *Journal of Structural Geology*, *28*(11), 1893–1908. https://doi.org/10.1016/j.jsg.2006.09.006

Carola, E., Tavani, S., Ferrer, O., Granado, P., Quintà, A., Butillé, M., & Muñoz, J. A. (2013). Along-strike extrusion at the transition between thin- and thick-skinned domains in the Pyrenean Orogen (northern Spain). *Geological Society, London, Special Publications*, *377*(1), 119–140. https://doi.org/10.1144/SP377.3

Carrera, N., & Muñoz, J. A. (2013). Thick-skinned tectonic style resulting from the inversion of previous structures in the southern Cordillera Oriental (NW Argentine Andes). *Geological Society, London, Special Publications*, *377*(1), 77–100. https://doi.org/10.1144/SP377.2

Chapple, W. M. (1978). Mechanics of thin-skinned fold-and-thrust belts. *GSA Bulletin*, *89*(8), 1189–1198. https://doi.org/10.1130/0016-7606(1978)89<1189:motfb>2.0.co;2

Charreau, J., Avouac, J.-P., Chen, Y., Dominguez, S., & Gilder, S. (2008). Miocene to present kinematics of fault-bend folding across the Huerguosi anticline, northern Tianshan (China), derived from structural, seismic, and magnetostratigraphic data. *Geology*, *36*(11), 871–874. https://doi.org/10.1130/G25073A.1

Charreau, J., Chen, Y., Gilder, S., Barrier, L., Dominguez, S., Augier, R., et al. (2009). Neogene uplift of the Tian Shan Mountains observed in the magnetic record of the Jingou River section (northwest China). *Tectonics*, *28*(2), TC2008. https://doi.org/10.1029/2007tc002137

Charreau, J., Chen, Y., Gilder, S., Dominguez, S., Avouac, J.-P., Sen, S., et al. (2005). Magnetostratigraphy and rock magnetism of the Neogene Kuitun He section (northwest China): Implications for late cenozoic uplift of the Tianshan mountains. *Earth and Planetary Science Letters*, *230*(1–2), 177–192. https://doi.org/10.1016/j.epsl.2004.11.002

Charreau, J., Gumiaux, C., Avouac, J.-P., Augier, R., Chen, Y., Barrier, L., et al. (2009). The Neogene Xiyu Formation, a diachronous prograding gravel wedge at front of the Tianshan: Climatic and tectonic implications. *Earth and Planetary Science Letters*, *287*(3), 298–310. https://doi.org/10.1016/j.epsl.2009.07.035

Charreau, J., Saint-Carlier, D., Lavé, J., Dominguez, S., Blard, P.-H., Avouac, J.-P., et al. (2018). Late Pleistocene acceleration of deformation across the northern Tianshan piedmont (China) evidenced from the morpho-tectonic evolution of the Dushanzi anticline. *Tectonophysics*, *730*, 132–140. https://doi.org/10.1016/j.tecto.2018.02.016

Chen, W., Hao, J. J., Li, S. Q., Peng, W. L., Xian, D., Chen, L. H., & Li, Z. G. (2012). The geometric and kinematic numerical simulation of the Dushanzi anticline, southern Junggar Basin. *Chinese Journal of Geology*, *47*, 37–50.

Chen, Z., Cao, Y., Wang, X., Qiu, L., Tang, Y., & Yuan, G. (2016). Oil origin and accumulation in the Paleozoic Chepaizi–Xinguang field, Junggar Basin, China. *Journal of Asian Earth Sciences*, *115*, 1–15. https://doi.org/10.1016/j.jseaes.2015.09.019

Choulet, F., Chen, Y., Wang, B., Faure, M., Cluzel, D., Charvet, J., et al. (2011). Late Paleozoic paleogeographic reconstruction of Western Central Asia based upon paleomagnetic data and its geodynamic implications. *Journal of Asian Earth Sciences*, *42*(5), 867–884. https://doi.org/10.1016/j.jseaes.2010.07.011

Cloos, H. (1928). *Experimenten zur inneren Tektonik* (p. 609). Centralblattfur Mineralogic and Paleontologie.

Cooper, M., Williams, G., Graciansky, P., Murphy, R., Needham, T., De Paor, D., et al. (1989). Inversion tectonics—A discussion. *Geological Society, London, Special Publications*, *44*(1), 335–347. https://doi.org/10.1144/GSL.SP.1989.044.01.18

Costa, E., & Vendeville, B. C. (2002). Experimental insights on the geometry and kinematics of fold-and-thrust belts above weak, viscous evaporitic décollement. *Journal of Structural Geology*, *24*(11), 1729–1739. https://doi.org/10.1016/S0191-8141(01)00169-9

Craddock, J. P., & van der Pluijm, B. A. (1989). Late Paleozoic deformation of the cratonic carbonate cover of eastern North America. *Geology*, *17*(5), 416–419. https://doi.org/10.1130/0091-7613(1989)017<0416:Lpdotc>2.3.Co;2

Daëron, M., Avouac, J.-P., & Charreau, J. (2007). Modeling the shortening history of a fault tip fold using structural and geomorphic records of deformation. *Journal of Geophysical Research*, *112*(B3), B03S12. https://doi.org/10.1029/2006JB004460

Dair, L., & Cooke, M. L. (2009). San Andreas Fault geometry through the San Gorgonio Pass, California. *Geology*, *37*(2), 119–122. https://doi.org/10.1130/g25101a.1

Davis, D. M., & Engelder, T. (1985). The role of salt in fold-and-thrust belts. *Tectonophysics*, *119*(1), 67–88. https://doi.org/10.1016/0040-1951(85)90033-2

Davis, G. H., Bump, A. P., García, P. E., & Ahlgren, S. G. (2000). Conjugate Riedel deformation band shear zones. *Journal of Structural Geology*, *22*(2), 169–190. https://doi.org/10.1016/S0191-8141(99)00140-6

De Grave, J., Buslov, M. M., & Van den haute, P. (2007). Distant effects of India–Eurasia convergence and Mesozoic intracontinental deformation in Central Asia: Constraints from apatite fission-track thermochronology. *Journal of Asian Earth Sciences*, *29*(2), 188–204. https://doi.org/10.1016/j.jseaes.2006.03.001

De Grave, J., De Pelsmaeker, E., Zhimulev, F. I., Glorie, S., Buslov, M. M., & Van den haute, P. (2014). Meso-Cenozoic building of the northern central Asian orogenic belt: Thermotectonic history of the Tuva region. *Tectonophysics*, *621*, 44–59. https://doi.org/10.1016/j.tecto.2014.01.039

De Grave, J., & Van den haute, P. (2002). Denudation and cooling of the lake Teletskoye region in the Altai mountains (South Siberia) as revealed by apatite fission-track thermochronology. *Tectonophysics*, *349*(1), 145–159. https://doi.org/10.1016/S0040-1951(02)00051-3

Di Domenica, A., Bonini, L., Calamita, F., Toscani, G., Galuppo, C., & Seno, S. (2014). Analogue modeling of positive inversion tectonics along differently oriented pre-thrusting normal faults: An application to the Central-Northern Apennines of Italy. *GSA Bulletin*, *126*(7–8), 943–955. https://doi.org/10.1130/b31001.1

Dong, Y., Zhang, M., Zhu, X., Jiang, Q., Guo, L., & Wei, M. (2017). Seismic geomorphology and depositional system of delta and terminal fan: A case study of the Neogene Shawan formation in the Chepaizi uplift, Junggar Basin, China. *Marine and Petroleum Geology*, *83*, 362–381. https://doi.org/10.1016/j.marpetgeo.2016.10.006

Dooley, T., & McClay, K. (1997). Analog modeling of pull-apart Basins1. *AAPG Bulletin*, *81*(11), 1804–1826. https://doi.org/10.1306/3b05c636-172a-11d7-8645000102c1865d

Dooley, T. P., & Schreurs, G. (2012). Analogue modelling of intraplate strike-slip tectonics: A review and new experimental results. *Tectonophysics*, *574–575*, 1–71. https://doi.org/10.1016/j.tecto.2012.05.030

Du, J., Zhi, D., Li, J., Yang, D., Tang, Y., Qi, X., et al. (2019). Major breakthrough of Well Gaotan 1 and exploration prospects of lower assemblage in southern margin of Junggar Basin, NW China. *Petroleum Exploration and Development*, *46*(2), 216–227. https://doi.org/10.1016/S1876-3804(1960003-0)

Dumitru, T. A., Zhou, D., Chang, E., Graham, S., Hendrix, M., Sobel, E., & Carroll, A. (2001). Uplift, exhumation, and deformation in the Chinese Tian Shan. *Geological Society of America Memoir*, *194*, 71–99. https://doi.org/10.1130/0-8137-1194-0.71

Eichelberger, N. W., Hughes, A. N., & Nunns, A. G. (2015). Combining multiple quantitative structural analysis techniques to create robust structural interpretations. *Interpretation*, *3*(4), SAA89–SAA104. https://doi.org/10.1190/INT-2015-0016.1

Elliott, A. J., Oskin, M. E., Liu-zeng, J., & Shao, Y. X. (2018). Persistent rupture terminations at a restraining bend from slip rates on the eastern Altyn Tagh fault. *Tectonophysics*, *733*, 57–72. https://doi.org/10.1016/j.tecto.2018.01.004

Emmons, R. C. (1969). Strike-slip rupture patterns in sand models. *Tectonophysics*, *7*(1), 71–87. https://doi.org/10.1016/0040-1951(69)90065-1

Engelder, T., & Engelder, R. (1977). Fossil distortion and décollement tectonics of the Appalachian Plateau. *Geology*, *5*(8), 457–460. https://doi.org/10.1130/0091-7613(1977)5<457:Fdadto>2.0.Co;2

Engelder, T., & Geiser, P. (1979). The relationship between pencil cleavage and lateral shortening within the Devonian section of the Appalachian Plateau, New York. *Geology*, *7*(9), 460–464. https://doi.org/10.1130/0091-7613(1979)7<460:Trbpca>2.0.Co;2

Erslev, E. A. (1991). Trishear fault-propagation folding. *Geology*, *19*(6), 617–620. https://doi.org/10.1130/0091-7613(1991)019<0617:tfpf>2.3.co;2

Gao, X., Liu, L., Jiang, Z., Shang, X., & Liu, G. (2013). A pre-Paleogene unconformity surface of the Sikeshu Sag, Junggar Basin: Lithological, geophysical and geochemical implications for the transportation of hydrocarbons. *Geoscience Frontiers*, *4*(6), 779–786. https://doi.org/10.1016/j.gsf.2012.12.003

Ghalayini, R., Daniel, J.-M., Homberg, C., Nader, F. H., & Comstock, J. E. (2014). Impact of Cenozoic strike-slip tectonics on the evolution of the northern Levant Basin (offshore Lebanon). *Tectonics*, *33*(11), 2121–2142. https://doi.org/10.1002/2014tc003574

Giambiagi, L., Bechis, F., García, V., & Clark, A. H. (2008). Temporal and spatial relationships of thick- and thin-skinned deformation: A case study from the Malargüe fold-and-thrust belt, southern central Andes. *Tectonophysics*, *459*(1), 123–139. https://doi.org/10.1016/j.tecto.2007.11.069

Glorie, S., & De Grave, J. (2016). Exhuming the Meso–cenozoic Kyrgyz Tianshan and Siberian Altai-Sayan: A review based on low-temperature thermochronology. *Geoscience Frontiers*, *7*(2), 155–170. https://doi.org/10.1016/j.gsf.2015.04.003

Glorie, S., De Grave, J., Buslov, M. M., Elburg, M. A., Stockli, D. F., Gerdes, A., & Van den haute, P. (2010). Multi-method chronometric constraints on the evolution of the Northern Kyrgyz Tien Shan granitoids (central Asian orogenic belt): From emplacement to exhumation. *Journal of Asian Earth Sciences*, *38*(3), 131–146. https://doi.org/10.1016/j.jseaes.2009.12.009

Gomez, F., Nemer, T., Tabet, C., Khawlie, M., Meghraoui, M., & Barazangi, M. (2007). Strain partitioning of active transpression within the Lebanese restraining bend of the Dead Sea Fault (Lebanon and SW Syria). *Geological Society, London, Special Publications*, *290*(1), 285–303. https://doi.org/10.1144/290.10

Granado, P., Roca, E., Strauss, P., Pelz, K., & Muñoz, J. A. (2018). Structural styles in fold-and-thrust belts involving early salt structures: The Northern Calcareous Alps (Austria). *Geology*, *47*(1), 51–54. https://doi.org/10.1130/G45281.1

Granado, P., & Ruh, J. B. (2019). Numerical modelling of inversion tectonics in fold-and-thrust belts. *Tectonophysics*, *763*, 14–29. https://doi.org/10.1016/j.tecto.2019.04.033

Guan, S., Stockmeyer, J. M., Shaw, J. H., Plesch, A., & Zhang, J. (2016). Structural inversion, imbricate wedging, and out-of-sequence thrusting in the southern Junggar fold-and-thrust belt, northern Tian Shan, China. *AAPG Bulletin*, *100*(9), 1443–1468. https://doi.org/10.1306/04041615023

Han, B.-F., Guo, Z.-J., Zhang, Z.-C., Zhang, L., Chen, J.-F., & Song, B. (2010). Age, geochemistry, and tectonic implications of a late Paleozoic stitching pluton in the North Tian Shan suture zone, western China. *GSA Bulletin*, *122*(3–4), 627–640. https://doi.org/10.1130/b26491.1

Heermance, R. V., Chen, J., Burbank, D. W., & Wang, C. (2007). Chronology and tectonic controls of Late Tertiary deposition in the southwestern Tian Shan foreland, NW China. *Basin Research*, *19*(4), 599–632. https://doi.org/10.1111/j.1365-2117.2007.00339.x

Hendrix, M. S. (2000). Evolution of Mesozoic sandstone Compositions, southern Junggar, northern Tarim, and western Turpan basins, northwest China: A detrital record of the Ancestral Tian Shan. *Journal of Sedimentary Research*, *70*(3), 520–532. https://doi.org/10.1306/2-Dc40924-0e47-11d7-8643000102c1865d

Hendrix, M. S., Graham, S. A., Carroll, A. R., Sobel, E. R., Mcknight, C. L., Schulein, B. J., & Wang, Z. (1992). Sedimentary record and climatic implications of recurrent deformation in the Tian Shan: Evidence from Mesozoic strata of the north Tarim, south Junggar, and Turpan basins, northwest China. *GSA Bulletin*, *104*(1), 53–79. https://doi.org/10.1130/0016-7606(1992)104<0053:sracio>2.3.co;2

Henry, P., Jouniaux, L., Screaton, E. J., Hunze, S., & Saffer, D. M. (2003). Anisotropy of electrical conductivity record of initial strain at the toe of the Nankai accretionary wedge. *Journal of Geophysical Research*, *108*(B9), 2407. https://doi.org/10.1029/2002JB002287

Hessami, K., Koyi, H. A., & Talbot, C. J. (2001). The significance of strike-slip faulting in the basement of the Zagros fold and thrust belt. *Journal of Petroleum Geology*, *24*(1), 5–28. https://doi.org/10.1111/J.1747-5457.2001.Tb00659.X

Homberg, C., Bergerat, F., Philippe, Y., Lacombe, O., & Angelier, J. (2002). Structural inheritance and cenozoic stress fields in the Jura fold-and-thrust belt (France). *Tectonophysics*, *357*(1), 137–158. https://doi.org/10.1016/S0040-1951(02)00366-9

Huang, B., Piper, J. D. A., Qiao, Q., Wang, H., & Zhang, C. (2010). Magnetostratigraphic and rock magnetic study of the Neogene upper Yaha section, Kuche Depression (Tarim Basin): Implications to formation of the Xiyu conglomerate formation, NW China. *Journal of Geophysical Research*, *115*(B1), B01101. https://doi.org/10.1029/2008JB006175

Jolivet, M. (2017). Mesozoic tectonic and topographic evolution of Central Asia and Tibet: A preliminary synthesis. *Geological Society, London, Special Publications*, *427*(1), 19–55. https://doi.org/10.1144/sp427.2

Jolivet, M., Barrier, L., Dauteuil, O., Laborde, A., Li, Q., Reichenbacher, B., et al. (2018). Late Cretaceous–Palaeogene topography of the Chinese Tian Shan: New insights from geomorphology and sedimentology. *Earth and Planetary Science Letters*, *499*, 95–106. https://doi.org/10.1016/j.epsl.2018.07.004

Jolivet, M., Brunel, M., Seward, D., Xu, Z., Yang, J., Roger, F., et al. (2001). Mesozoic and Cenozoic tectonics of the northern edge of the Tibetan plateau: Fission-track constraints. *Tectonophysics*, *343*(1), 111–134. https://doi.org/10.1016/S0040-1951(01)00196-2

Jolivet, M., Dominguez, S., Charreau, J., Chen, Y., Li, Y., Wang, Q., & Jolivet, C. (2010). Mesozoic and Cenozoic tectonic history of the Central Chinese Tian Shan: Reactivated tectonic structures and active deformation. *Tectonics*, *29*(6), 1–30. https://doi.org/10.1029/2010TC002712

Kapp, P., Pg, D., Ge, G., Heizler, M., & Ding, L. (2007). Geological records of the Lhasa-Qiangtang and Indo-Asian collisions in the Nima area of central Tibet. *Geological Society of America Bulletin*, *119*, 917–932. https://doi.org/10.1130/B26033

Koyi, H. A., Sans, M., Teixell, A., Cotton, J., & Zeyen, H. (2004). The significance of penetrative strain in the restoration of shortened layers—Insights from sand models and the Spanish Pyrenees.

Krzywiec, P., Gągała, Ł., Mazur, S., Słonka, Ł., Kufrasa, M., Malinowski, M., et al. (2017). Variscan deformation along the Teisseyre-Tornquist Zone in SE Poland: Thick-skinned structural inheritance or thin-skinned thrusting. *Tectonophysics*, *718*, 83–91. https://doi.org/10.1016/j.tecto.2017.06.008

Lacombe, O., & Bellahsen, N. (2016). Thick-skinned tectonics and basement-involved fold–thrust belts: Insights from selected Cenozoic orogens. *Geological Magazine*, *153*(5–6), 763–810. https://doi.org/10.1017/s0016756816000078

Laurent, A., Averbuch, O., Beccaletto, L., Graveleau, F., Lacquement, F., Capar, L., & Marc, S. (2021). 3-D structure of the variscan thrust front in Northern France: New Insights from Seismic Reflection Profiles. *Tectonics*, *40*(7), e2020TC006642. https://doi.org/10.1029/2020TC006642

Laurent-Charvet, S., Charvet, J., Shu, L., Ma, R., & Lu, H. (2002). Palaeozoic late collisional strike-slip deformations in Tianshan and Altai, Eastern Xinjiang, NW China. *Terra Nova*, *14*(4), 249–256. https://doi.org/10.1046/j.1365-3121.2002.00417.x

Le Pichon, X., & Gaulier, J. M. (1988). The rotation of Arabia and the Levant fault system. *Tectonophysics*, *153*(1–4), 271–294. https://doi.org/10.1016/0040-1951(88)90020-0

Li, Z., Chen, W., Jia, D., Sun, C., Zheng, W., Zhang, P., et al. (2020). The effects of fault geometry and kinematic parameters on 3-D fold morphology: Insights from 3-D geometric models and comparison with the Dushanzi Anticline, China. *Tectonics*, *39*(2), e2019TC005713. https://doi.org/10.1029/2019tc005713

Lu, H., Burbank, D., Li, Y., & Liu, Y. (2009). Late Cenozoic structural and stratigraphic evolution of the northern Chinese Tian Shan foreland. *Basin Research*, *22*(3), 249–269. https://doi.org/10.1111/j.1365-2117.2009.00412.x

Lu, H., Li, B., Wu, D., Zhao, J., Zheng, X., Xiong, J., & Li, Y. (2019). Spatiotemporal patterns of the Late Quaternary deformation across the northern Chinese Tian Shan foreland. *Earth-Science Reviews*, *194*, 19–37. https://doi.org/10.1016/j.earscirev.2019.04.026

Lu, R. Q., He, D. F., Xu, X. W., Wang, X. S., Tan, X. B., & Wu, X. Y. (2018). Seismotectonics of the 2016 M 6.2 Hutubi Earthquake: Implications for the 1906 M 7.7 Manas Earthquake in the Northern Tian Shan Belt, China. *Seismological Research Letters*, *89*(1), 13–21. https://doi.org/10.1785/0220170123

Luo, X., Wang, Z., Zhang, L., Yang, W., & Liu, L. (2007). Overpressure generation and evolution in a compressional tectonic setting, the southern margin of Junggar Basin, northwestern China. *AAPG Bulletin*, *91*(8), 1123–1139. https://doi.org/10.1306/02260706035

Ma, X., Shu, L., & Meert, J. G. (2015). Early Permian slab breakoff in the Chinese Tianshan belt inferred from the post-collisional granitoids. *Gondwana Research*, *27*(1), 228–243. https://doi.org/10.1016/j.gr.2013.09.018

Macaulay, E. A., Sobel, E. R., Mikolaichuk, A., Kohn, B., & Stuart, F. M. (2014). Cenozoic deformation and exhumation history of the Central Kyrgyz Tien Shan. *Tectonics*, *33*(2), 135–165. https://doi.org/10.1002/2013TC003376

Madritsch, H., Schmid, S. M., & Fabbri, O. (2008). Interactions between thin- and thick-skinned tectonics at the northwestern front of the Jura fold-and-thrust belt (eastern France). *Tectonics*, *27*(5), TC5005. https://doi.org/10.1029/2008TC002282

Malz, A., Madritsch, H., Jordan, P., Meier, B., & Kley, J. (2020). Along-strike variations in thin-skinned thrusting style controlled by pre-existing basement structure in the easternmost Jura Mountains (Northern Switzerland). *Geological Society, London, Special Publications*, *490*(1), 199–220. https://doi.org/10.1144/SP490-2019-090

Mann, P., Burke, K., & Matumoto, T. (1984). Neotectonics of Hispaniola: Plate motion, sedimentation, and seismicity at a restraining bend. *Earth and Planetary Science Letters*, *70*(2), 311–324. https://doi.org/10.1016/0012-821X(84)90016-5

McClay, K., & Bonora, M. (2001). Analog Models of Restraining Stepovers in Strike-Slip Fault Systems. *AAPG Bulletin*, *85*(2), 233–260. https://doi.org/10.1306/8626c7ad-173b-11d7-8645000102c1865d

McClay, K., & Dooley, T. (1995). Analogue models of pull-apart basins. *Geology*, *23*(8), 711–714. https://doi.org/10.1130/0091-7613(1995)023<0711:amopab>2.3.co;2

McClay, K. R. (1992). Glossary of thrust tectonics terms. *Thrust tectonics*, 419–433.
Medwedeff, D. (1990). Geometry and kinematics of an active, laterally propagating wedge-thrust, Wheeler Ridge, California. *AAPG Bulletin*, *74*(5), 921–945. https://doi.org/10.1306/44B4B61C-170A-11D7-8645000102C1865D
Miller, M. G. (2003). Basement-involved thrust faulting in a thin-skinned fold-and-thrust belt. *Death Valley, California, USA, Geology*, *31*(1), 31–34. https://doi.org/10.1130/0091-7613(2003)031<0031:bitfia>2.0.co;2
Molinaro, M., Leturmy, P., Guezou, J.-C., Frizon de Lamotte, D., & Eshraghi, S. A. (2005). The structure and kinematics of the southeastern Zagros fold-thrust belt, Iran: From thin-skinned to thick-skinned tectonics. *Tectonics*, *24*(3), TC3007. https://doi.org/10.1029/2004TC001633
Molnar, P., Brown, E. T., Burchfiel, B. C., Deng, Q., Feng, X., Li, J., et al. (1994). Quaternary climate change and the formation of river terraces across growing anticlines on the north flank of the Tien Shan, China. *The Journal of Geology*, *102*(5), 583–602. https://doi.org/10.1086/629700
Molnar, P., & Ghose, S. (2000). Seismic moments of major earthquakes and the rate of shortening across the Tien Shan. *Geophysical Research Letters*, *27*(16), 2377–2380. https://doi.org/10.1029/2000GL011637
Morin, J., Jolivet, M., Shaw, D., Bourquin, S., & Bataleva, E. (2020). New sedimentological and palynological data from the Yarkand-Fergana Basin (Kyrgyz Tian Shan): Insights on its Mesozoic paleogeographic and tectonic evolution. *Geoscience Frontiers*, *12*(1), 183–202. https://doi.org/10.1016/j.gsf.2020.04.010
Mouthereau, F., & Lacombe, O. (2006). Inversion of the Paleogene Chinese continental margin and thick-skinned deformation in the Western Foreland of Taiwan. *Journal of Structural Geology*, *28*(11), 1977–1993. https://doi.org/10.1016/j.jsg.2006.08.007
Mouthereau, F., Tensi, J., Bellahsen, N., Lacombe, O., De Boisgrollier, T., & Kargar, S. (2007). Tertiary sequence of deformation in a thin-skinned/thick-skinned collision belt: The Zagros Folded Belt (Fars, Iran). *Tectonics*, *26*(5), TC5006. https://doi.org/10.1029/2007TC002098
Nilforoushan, F., Koyi, H. A., Swantesson, J. O. H., & Talbot, C. J. (2008). Effect of basal friction on surface and volumetric strain in models of convergent settings measured by laser scanner. *Journal of Structural Geology*, *30*(3), 366–379. https://doi.org/10.1016/j.jsg.2007.09.013
Novikov, I. S. (2013). Reconstructing the stages of orogeny around the Junggar basin from the lithostratigraphy of Late Paleozoic, Mesozoic, and Cenozoic sediments. *Russian Geology and Geophysics*, *54*(2), 138–152. https://doi.org/10.1016/j.rgg.2013.01.002
Pfiffner, O. A. (2017). Thick-Skinned and Thin-Skinned Tectonics: A Global Perspective. *Geosciences*, *7*(3), 71. https://doi.org/10.3390/geosciences7030071
Philippe, Y., Deville, E., & Mascle, A. (1998). Thin-skinned inversion tectonics at oblique basin margins: Example of the western Vercors and Chartreuse Subalpine massifs (SE France). *Geological Society, London, Special Publications*, *134*(1), 239–262. https://doi.org/10.1144/GSL.SP.1998.134.01.11
Poisson, B., & Avouac, J.-P. (2004). Holocene Hydrological Changes Inferred from Alluvial Stream Entrenchment in North Tian Shan (Northwestern China). *The Journal of Geology*, *112*(2), 231–249. https://doi.org/10.1086/381659
Qiao, Q., Huang, B., Piper, J. D. A., Deng, T., & Liu, C. (2016). Neogene magnetostratigraphy and rock magnetic study of the Kashi Depression, NW China: Implications to neotectonics in the SW Tianshan Mountains. *Journal of Geophysical Research: Solid Earth*, *121*(3), 1280–1296. https://doi.org/10.1002/2015JB012687
Qiu, J., Rao, G., Wang, X., Yang, D., & Xiao, L. (2019). Effects of fault slip distribution on the geometry and kinematics of the southern Junggar fold-and-thrust belt, northern Tian Shan. *Tectonophysics*, *772*, 228209. https://doi.org/10.1016/j.tecto.2019.228209
Ravaglia, A., Seno, S., Toscani, G., & Fantoni, R. (2006). Mesozoic extension controlling the Southern Alps thrust front geometry under the Po Plain, Italy: Insights from sandbox models. *Journal of Structural Geology*, *28*(11), 2084–2096. https://doi.org/10.1016/j.jsg.2006.07.011
Richard, P. D., Naylor, M. A., & Koopman, A. (1995). Experimental models of strike-slip tectonics. *Petroleum Geoscience*, *1*(1), 71–80. https://doi.org/10.1144/petgeo.1.1.71
Riedel, W. (1929). Zur Mechanik geologischer Brucherscheinungen ein Beitrag zum Problem der Fiederspatten. In *Zentralblatt fur Mineralogie, Geologie und Paleontologie Abt.* (pp. 354–368).
Ruh, J. B., & Vergés, J. (2018). Effects of reactivated extensional basement faults on structural evolution of fold-and-thrust belts: Insights from numerical modelling applied to the Kopet Dagh Mountains. *Tectonophysics*, *746*, 493–511. https://doi.org/10.1016/j.tecto.2017.05.020
Sans, M., Vergés, J., Gomis, E., Parés, J. M., Schiattarella, M., Travé, A., et al. (2003). Layer parallel shortening in salt-detached folds: Constraint on cross-section restoration. *Tectonophysics*, *372*(1), 85–104. https://doi.org/10.1016/S0040-1951(03)00233-6
Schedl, A., & Wiltschko, D. V. (1987). Possible effects of pre-existing basement topography on thrust fault ramping. *Journal of Structural Geology*, *9*(8), 1029–1037. https://doi.org/10.1016/0191-8141(87)90011-3
Schori, M., Zwaan, F., Schreurs, G., & Mosar, J. (2021). Pre-existing basement faults controlling deformation in the Jura mountains fold-and-thrust belt: Insights from analogue models. *Tectonophysics*, *814*, 228980. https://doi.org/10.1016/j.tecto.2021.228980
Schwartz, S. Y., Orange, D. L., & Anderson, R. S. (1990). Complex fault interactions in a restraining bend on the San Andreas Fault, southern Santa Cruz Mountains, California. *Geophysical Research Letters*, *17*(8), 1207–1210. https://doi.org/10.1029/gl017i008p01207
Scisciani, V. (2009). Styles of positive inversion tectonics in the Central Apennines and in the Adriatic foreland: Implications for the evolution of the Apennine chain (Italy). *Journal of Structural Geology*, *31*(11), 1276–1294. https://doi.org/10.1016/j.jsg.2009.02.004
Segall, P., & Pollard, D. D. (1980). Mechanics of discontinuous faults. *Journal of Geophysical Research*, *85*(B8), 4337–4350. https://doi.org/10.1029/JB085iB08p04337
Selander, J., Oskin, M., Ormukov, C., & Abdrakhmatov, K. (2012). Inherited strike-slip faults as an origin for basement-cored uplifts: Example of the Kungey and Zailiskey ranges, northern Tian Shan. *Tectonics*, *31*(4), 561. https://doi.org/10.1029/2011TC003002
Shaw, J. H., Connors, C., & Suppe, J. (2005). Seismic interpretation of contractional fault-related folds. *American Association of Petroleum Geologists*, *53*. https://doi.org/10.1306/St531003
Shen, Z., Yu, F., Wang, Q., Zhang, J., & Xue, Y. (2022). Discrete element method simulation of the fold-and-thrust belts along strike various compression in the southern margin of the Junggar Basin, China. *Marine and Petroleum Geology*, *145*, 105849. https://doi.org/10.1016/j.marpetgeo.2022.105849
Shu, L. S., Charvet, J., Guo, L. Z., Lu, H. F., & Laurent-Charvet, S. (1999). A large-scale Palaeozoic dextral ductile strike-slip zone: The Aqqikkudug-Weiya zone along the northern margin of the Central Tianshan belt, Xinjiang, NW China. *Acta Geologica Sinica-English Edition*, *73*(2), 148–162. https://doi.org/10.1111/j.1755-6724.1999.tb00822.x
Sobel, E. R., Chen, J., & Heermance, R. V. (2006). Late Oligocene-Early Miocene initiation of shortening in the Southwestern Chinese Tian Shan: Implications for Neogene shortening rate variations. *Earth and Planetary Science Letters*, *247*(1), 70–81. https://doi.org/10.1016/j.epsl.2006.03.048
Stockmeyer, J. M., Shaw, J. H., & Guan, S. (2014). Seismic hazards of multisegment thrust-fault ruptures: Insights from the 1906 Mw 7.4–8.2 Manas, China, earthquake. *Seismological Research Letters*, *85*(4), 801–808. https://doi.org/10.1785/0220140026
StructureSolver LLC, 2009–2019. (2022). StructureSolver User Workshop (Version 1) [Dataset]. Figshare. https://doi.org/10.6084/m9.figshare.20444976.v1

Su, P., He, H., Wei, Z., Lu, R., Shi, F., Sun, H., et al. (2018). A new shortening rate across the Dushanzi anticline in the northern Tian Shan Mountains, china from lidar data and a seismic reflection profile. *Journal of Asian Earth Sciences*, *163*, 131–141. https://doi.org/10.1016/j.jseaes.2018.06.008

Sun, J., Zhu, R., & Bowler, J. (2004). Timing of the Tianshan Mountains uplift constrained by magnetostratigraphic analysis of molasse deposits. *Earth and Planetary Science Letters*, *219*(3), 239–253. https://doi.org/10.1016/S0012-821X(04)00008-1

Suppe, J. (1983). Geometry and kinematics of fault-bend folding. *American Journal of Science*, *283*(7), 684–721. https://doi.org/10.2475/ajs.283.7.684

Suppe, J., Chou, G. T., & Hook, S. C. (1992). Rates of folding and faulting determined from growth strata. In K. R. McClay (Ed.) *Thrust tectonics* (pp. 105–121). Springer Netherlands. https://doi.org/10.1007/978-94-011-3066-0_9

Suppe, J., Connors, C. D., & Zhang, Y. (2004). Shear fault-bend folding. In K. R. McClay (Ed.), *Thrust tectonics and hydrocarbon systems: AAPG memoir 82* (pp. 303–323). https://doi.org/10.1306/m82813c17

Suppe, J., & Medwedeff, D. A. (1990). Geometry and kinematics of fault-propagation folding. *Eclogae Geologicae Helvetiae*, *83*(3), 409–454.

Sylvester, A. G. (1988). Strike-slip faults. *GSA Bulletin*, *100*(11), 1666–1703. https://doi.org/10.1130/0016-7606(1988)100<1666:ssf>2.3.co;2

Tan, C., Yu, X., Li, S., Shan, X., & Chen, B. (2016). Sedimentology and stratigraphic evolution of the fan delta at the Badaowan formation (lower Jurassic), Southern Junggar Basin, Northwest China. *Arabian Journal of Geosciences*, *9*(2), 115. https://doi.org/10.1007/s12517-015-2242-4

Tavarnelli, E., Butler, R., Decandia, F., Calamita, F., Grasso, M., Alvarez, W., et al. (2004). Implications of fault reactivation and structural inheritance in the Cenozoic tectonic evolution of Italy. In *The geology of Italy, special, 1* (pp. 209–222).

Tchalenko, J. S. (1970). Similarities between shear zones of different magnitudes. *GSA Bulletin*, *81*(6), 1625–1640. https://doi.org/10.1130/0016-7606(1970)81[1625:sbszod]2.0.co;2

Thompson Jobe, J. A., Li, T., Bookhagen, B., Chen, J., & Burbank, D. (2018). Dating growth strata and basin fill by combining $^{26}Al/^{10}Be$ burial dating and magnetostratigraphy: Constraining active deformation in the Pamir–Tian Shan convergence zone, NW China. *Lithosphere*, *10*(6), 806–828. https://doi.org/10.1130/l727.1

Van der Voo, R., Levashova, N. M., Skrinnik, L. I., Kara, T. V., & Bazhenov, M. L. (2006). Late orogenic, large-scale rotations in the Tien Shan and adjacent mobile belts in Kyrgyzstan and Kazakhstan. *Tectonophysics*, *426*(3), 335–360. https://doi.org/10.1016/j.tecto.2006.08.008

Vincent, S., & Allen, M. (2001). Sedimentary record of Mesozoic intracontinental deformation in the eastern Junggar Basin, northwest China: Response to orogeny at the Asian margin. *Memoir of the Geological Society of America*, *194*, 341–360. https://doi.org/10.1130/0-8137-1194-0.341

Walker, J. D., Geissman, J. W., Bowring, S. A., & Babcock, L. E. (2013). The Geological Society of America geologic time scale. *Bulletin*, *125*(3–4), 259–272. https://doi.org/10.1130/B30712.1

Wan, Z., Shi, Q., Zhang, Q., Cai, S., & Xia, B. (2015). Characteristics and developmental mechanisms of mud volcanoes on the southern margin of the Junggar Basin, NW China. *Geological Journal*, *50*(4), 434–445. https://doi.org/10.1002/gj.2547

Wang, Y., Jia, D., Zhang, H., Yuan, B., Wang, H., Wei, C., et al. (2020). Spatial and temporal associations of traps and sources: Insights into exploration in the southern Junggar foreland basin, northwestern China. *Journal of Asian Earth Sciences*, *198*, 104078. https://doi.org/10.1016/j.jseaes.2019.104078

Wang, Z., Zhi, D., Zhang, C., Xue, X., Zhang, S., Li, T., et al. (2009). Oil source analysis of Upper Tertiary Shawan Formation in Chepaizi area, in the northwest margin of Junggar basin. *Science in China Series D: Earth Sciences*, *52*(1), 106–114. https://doi.org/10.1007/s11430-009-5013-9

Weil, A. B., & Yonkee, A. (2009). Anisotropy of magnetic susceptibility in weakly deformed red beds from the Wyoming salient, Sevier thrust belt: Relations to layer-parallel shortening and orogenic curvature. *Lithosphere*, *1*(4), 235–256. https://doi.org/10.1130/l42.1

Whitaker, A. E., & Bartholomew, M. J. (1999). Layer parallel shortening; a mechanism for determining deformation timing at the junction of the Central and Southern Appalachians. *American Journal of Science*, *299*(3), 238–254. https://doi.org/10.2475/ajs.299.3.238

Wilhem, C., Windley, B. F., & Stampfli, G. M. (2012). The Altaids of Central Asia: A tectonic and evolutionary innovative review. *Earth-Science Reviews*, *113*(3–4), 303–341. https://doi.org/10.1016/j.earscirev.2012.04.001

Williams, G. D., Powell, C. M., & Cooper, M. A. (1989). Geometry and kinematics of inversion tectonics. *Geological Society, London, Special Publications*, *44*(1), 3–15. https://doi.org/10.1144/GSL.SP.1989.044.01.02

Wiltschko, D. V., Medwedeff, D. A., & Millson, H. E. (1985). Distribution and mechanisms of strain within rocks on the northwest ramp of Pine Mountain block, southern Appalachian foreland: A field test of theory. *GSA Bulletin*, *96*(4), 426–435. https://doi.org/10.1130/0016-7606(1985)96<426:Damosw>2.0.Co;2

Windhoffer, G., Bada, G., Nieuwland, D., Wórum, G., Horváth, F., & Cloetingh, S. (2005). On the mechanics of basin formation in the Pannonian basin: Inferences from analogue and numerical modelling. *Tectonophysics*, *410*(1–4), 389–415. https://doi.org/10.1016/j.tecto.2004.10.019

Windley, B. F., Alexeiev, D., Xiao, W., Kröner, A., & Badarch, G. (2007). Tectonic models for accretion of the Central Asian Orogenic Belt. *Journal of the Geological Society*, *164*(1), 31–47. https://doi.org/10.1144/0016-76492006-022

Wu, J. E., McClay, K., Whitehouse, P., & Dooley, T. (2009). 4D analogue modelling of transtensional pull-apart basins. *Marine and Petroleum Geology*, *26*(8), 1608–1623. https://doi.org/10.1016/j.marpetgeo.2008.06.007

Xiao, Q., Yu, G., Liu-Zeng, J., Oskin, M. E., & Shao, G. (2017). Structure and geometry of the Aksay restraining double bend along the Altyn Tagh Fault, northern Tibet, imaged using magnetotelluric method. *Geophysical Research Letters*, *44*(9), 4090–4097. https://doi.org/10.1002/2017gl072581

Yang, D., Xiao, L., Yan, G., Lingyun, W., Xin, W., & Xinqiang, W. (2019). Structural Characteristics and Petroleum Exploration in Sikeshu sag, southern margin of Junggar Basin. *Xinjing Petroleum Geology*, *40*, 138–144.

Yang, W., Dupont-Nivet, G., Jolivet, M., Guo, Z., Bougeois, L., Bosboom, R., et al. (2015). Magnetostratigraphic record of the early evolution of the southwestern Tian Shan foreland basin (Ulugqat area), interactions with Pamir indentation and India–Asia collision. *Tectonophysics*, *644–645*, 122–137. https://doi.org/10.1016/j.tecto.2015.01.003

Yang, W., Jolivet, M., Dupont-Nivet, G., Guo, Z., Zhang, Z., & Wu, C. (2013). Source to sink relations between the Tian Shan and Junggar Basin (northwest China) from Late Palaeozoic to Quaternary: Evidence from detrital U-Pb zircon geochronology. *Basin Research*, *25*(2), 219–240. https://doi.org/10.1111/j.1365-2117.2012.00558.x

Yu, F., Li, X., Li, D., Feng, Z., & Li, X. (2012). Simulation for the controlling factors of structural deformation in the southern margin of the Junggar Basin. *Acta Geologica Sinica-English Edition*, *86*(4), 842–853. https://doi.org/10.1111/j.1755-6724.2012.00710.x

Yu, Y. L., Wang, X., Rao, G., & Wang, R. F. (2016). Mesozoic reactivated transpressional structures and multi-stage tectonic deformation along the Hong-Che fault zone in the northwestern Junggar Basin, NW China. *Tectonophysics*, *679*, 156–168. https://doi.org/10.1016/j.tecto.2016.04.039

Zhou, X. (1994). interpretation of seismic velocity anormaly in southern margin of junggar basin. *Xinjing Petroleum Geology*, *15*(1), 16–21.

Zhu, M., Liang, Z., Wang, X., Wang, R., Yu, Y., Xiao, L., & Wei, L. (2023). Mesozoic strike-slip fault system at the margin of the Junggar Basin, NW China. *Journal of Structural Geology*, *175*, 104950. https://doi.org/10.1016/j.jsg.2023.104950

Ziegler, P. A. (1989). Geodynamic model for Alpine intra-plate compressional deformation in Western and Central Europe. *Geological Society, London, Special Publications*, *44*(1), 63–85. https://doi.org/10.1144/GSL.SP.1989.044.01.05

Zorin, Y. A. (1999). Geodynamics of the western part of the Mongolia–Okhotsk collisional belt, Trans-Baikal region (Russia) and Mongolia. *Tectonophysics*, *306*(1), 33–56. https://doi.org/10.1016/S0040-1951(99)00042-6

References From the Supporting Information

Boyer, S. E., & Elliot, D. (1982). Thrust systems: Bulletin American association of petroleum geologists (Vol. *66*).

Medwedeff, D. (1992). Geometry and kinematics of an active, laterally propagating wedge thrust, Wheeler ridge, California (pp. 3–28).